January 2020

Study Of Grain Growth In Single-Phase Polycrystals

Pawan Vedanti
Wayne State University

STUDY OF GRAIN GROWTH IN SINGLE-PHASE POLYCRYSTALS

by

PAWAN VEDANTI

DISSERTATION

Submitted to the Graduate School

of Wayne State University,

Detroit, Michigan

in partial fulfillment of the requirements

for the degree of

DOCTOR OF PHILOSOPHY

2020

MAJOR: MECHANICAL ENGINEERING

Approved By:

_____

Advisor Date

_____

Advisor Date

_____

_____

_____

DEDICATION

This work is dedicated to my parents

who always encouraged me to ask questions

and my teachers who showed me the way to find answers.

ACKNOWLEDGEMENT

First and foremost, I am thankful to my professors, Dr. Victor Berdichevsky and Dr. Xin Wu for helping me understand new concepts in fundamental mathematics and engineering which have changed my perspective about science and research. After this experience, I appreciate the value of sincerity, punctuality and detailing more when it comes to learning anything.

The truth is I cannot have achieved this without a strong support group. I would like to thank everyone who has helped me along the way.

Special thanks to all the people who said “No” at the right moment and motivating me work harder for it.

TABLE OF CONTENTS

LIST OF FIGURES

LIST OF TABLES

INTRODUCTION

The main objective of this thesis is to get an in-depth understanding of the thermodynamic and topological characteristics of grain growth. This involves studying the entropy of grain structure, statistical characteristics of areas and perimeters of grains in 2D slices of polycrystals, and their evolution during grain growth. These characteristics were obtained by hand-tracing each grain boundary of the microstructure images. The process of grain growth has been examined for commercially pure nickel, AZ31b magnesium and Al 5083f aluminum. A comprehensive account of all the materials used and the experimental methods executed in this study has also been provided. The major results are as follows:

1. The evolution of entropy of grain structure per one grain, S_m^*, was studied experimentally. It fluctuates around an average value of 1.4.

$$S_m^* = -\sum p_i \, log \, p_i \approx 1 \cdot 4. \tag{1}$$

where for any given microstructure, probabilities p_i are interpreted in the following way: the possible values of grain sizes are split in bins and p_i is the portion of grains in the i^{th} bin.

2. Formula (1) is confusing because in general one could expect that microstructure entropy per unit volume, S_m, is a function of two variables, average 3D grain boundary area, a, and average grain volume, $\bar{v}$. The formula for entropy per unit volume,

$$S_m = S_m^* \, / \, \bar{v}. \tag{2}$$

indicates that S_m degenerates and is a function of only one variable, $\bar{v}$. Further investigation of this issue in terms of statistical characteristics, average grain perimeter and average grain area of all microstructures studied, resulted in an unexpected by-product: a relationship between average grain perimeter and average grain area,

$$\bar{p} = (3.97 \pm 0.04)\sqrt{\bar{a}}. \tag{3}$$

where $\bar{p}$ and $\bar{a}$ are the average perimeter and area of the grain boundary structure.

3. A natural consequence of (1) and (2) was the decay of total entropy,

$$\mathbb{S}_m = NS_m^*. \tag{4}$$

where $\mathbb{S}_m$ is the total microstructure entropy, N is the total number of grains and S_m^* is the entropy of grain structure per one grain.

4. During grain growth, an initially random structure achieves a steady-state by dissipating energy. This dissipative system and its related thermodynamics are studied using a modified Hillert type approach. The following two equations are derived for probability distribution of normalized grain area and normalized grain perimeters in any grain structure:

$$f\left(\frac{p}{\bar{p}}\right) = c_1 e^{-\check{z}\frac{p}{\bar{p}}}\left[e^{-\check{\zeta}k\varkappa\left(\frac{p}{\bar{p}}\right)^2} - e^{-\check{\zeta}\varkappa\left(\frac{p}{\bar{p}}\right)^2}\right]. \tag{5}$$

$$f\left(\frac{a}{\bar{a}}\right) = c_2 e^{-\check{\zeta}\frac{a}{\bar{a}}}\left[e^{-\check{z}\sqrt{\varkappa}\sqrt{\frac{a}{\bar{a}}}} - e^{-\check{z}\sqrt{\frac{\varkappa}{k}}\sqrt{\frac{a}{\bar{a}}}}\right]. \tag{6}$$

where $\frac{p}{\bar{p}}$ is perimeter of individual grain normalized by the mean perimeter, $\frac{a}{\bar{a}}$ is the area of individual grains normalized by mean area, k and $\varkappa$ are fitting parameters calculated by quantifying the shape of grains and c_1 and c_2 are normalizing constants. The evolution of the two parameters in the distribution equations has also been studied.

The layout of this thesis is as follows: An overview of the subject matter has been given in chapter 2, entropy decay during grain growth has been checked in chapter 3, grain growth experiments conducted have been explained in detail in chapter 4 to assist reproduction of experimental results, a 2D statistical model containing two new characteristics of grain structure in single-phase metals and alloys is suggested in chapter 5. Appendix A and B have microstructure data and images to support findings in chapter 3. Derivation of equations (5) and (6) is given in appendix C. Plots to show the correlation of derived equations with experimental data are shown in appendix D.

OVERVIEW

During solidification of pure metals, different cooling rates result in the varied structure of materials. If the metal is quenched at a very rapid rate, it usually results in a disordered arrangement of atoms[3]. These materials were earlier called "metallic glasses" but "amorphous solids" is considered a more appropriate term nowadays. If the cooling rate is relatively slow, polycrystals are formed. Polycrystals are materials that consist of many grains of different sizes. These individual grains are connected to each other by means of grain boundaries. In pure metals and single-phase alloys, the only difference between any two given grains would be the orientation in which their atoms are arranged. Grain boundaries are the void spaces in between two grains which are usually a few atomic diameters thick. Over this region, a state of disorder exists as the atoms on one end are oriented differently compared to the other[5]. Broadly, grain boundaries are classified as low angle and high angle grain boundaries based on the difference of angle between the orientation of the two grains. When a deformed material which contains dislocations and grains is annealed, the microstructure may lower its energy by recovery, recrystallization, or grain growth. The path chosen by the material depends on the temperature and time of annealing.

During recovery, there is a reduction of internal strain energy and there are no significant changes in the grain structure whereas recrystallization is characterized by the appearance of non-homogeneous small strain-free grains which make the material more ductile and soft[62]. Recovery is indicated by reduction of the total energy of the dislocation network by reducing the dislocation density. This happens in one of the following ways: grain boundaries and free surfaces act as a sink for the dislocations,

dislocations climb and if they are of opposite signs annihilate. This may sometimes lead to dislocations of one sign being accumulated locally in the metal. Some observations show that they arrange to form a low angle grain boundary. The edge and screw type of dislocation will form tilt and twist grain boundaries, respectively. Earlier studies have shown that the rate of recovery is directly proportional to strain-induced in cold-rolled metals[15]-[17], and large strain deformation leads to reduced thermal stability[18],[19], which has to be taken into account. Higher the prior deformation, higher is the stored energy and hence higher is the driving force. The driving force here refers to the global thermodynamic driving force. Recovery is, therefore, an important mechanism since it can take place at a low temperature. Basically, recovery involves all the processes which do not require high angle grain boundary movement as that is the main indicator of the start of recrystallization.

Recrystallization simply means that a set of new defect-free grains take over the entire microstructure until the material is fully covered. The driving force for this process is also the reduction of strain energy associated with dislocations[5]-[7]. This can sometimes lead to a non-uniform distribution of sizes if some grains have a preference to grow over others. Single crystal aluminum was deformed and annealed to observe the resulting grain growth. It was seen that a small number of sub-grains grow rapidly and "discontinuously" to large diameters. This phenomenon is also called abnormal grain growth[1]. Nucleation of new crystals takes place at the grain boundaries with high misorientation but that is not a sufficient condition to make sure that the recrystallized grain grows. The sub grain size is another important characteristic which decides the final size of the grain[84].

The main parameters which affect the energy of recovery and recrystallization are initial dislocation density, initial grain size, and temperature of annealing. Temperature of cold work, initial texture, GBCD, secondary particle density, secondary particle distribution, etc. are some of the other parameters which also have a contribution in the final microstructure obtained after annealing.

Grain growth occurs as some larger grains tend to "eat up" the smaller adjacent grains to grow. The major driving force for grain growth is the reduction of total area of grain boundary surfaces. There are many physical factors which affect this process such as temperature, time, type of annealing, the type of grain boundary and secondary (and/or tertiary) particle distribution to name a few. The soap froth analogy is the most used to explain the changes pertaining to grain boundaries when annealed. The difference between the two cases of soap froth and grain boundary motion is that mass flow of air is allowed within each cell of the froth to lower the curvature driving pressure whereas in grain growth, there is no possibility of rapid mass flow[55]. Grain boundary character distribution (GBCD) is the study of five macroscopic parameters (lattice angle in 3D and 2 boundary plane orientation vectors). GBCD of commercially pure Al is relatively isotropic with a large population of low angle grain boundaries. This can be attributed to the fact that the sample was annealed for 60 mins at 400 °C which created an equiaxed microstructure. Grain growth can be broadly classified into two types: "Normal" and "Abnormal". Normal or "continuous" grain growth is identified by the existence of a universal probability distribution of the relative grain sizes.

All the processes (recovery, recrystallization and grain growth) can occur simultaneously as well as in succession thus making it a difficult task to mark a clear

start and stop points for them. With advancements in microscopy, it has been possible to observe changes in the microstructure in more detail and it is seen that traditional classification of the annealing process into these three stages is not sufficient[85]-[92]. A variation in the number or arrangement of grains in metals will result in a change in the mechanical behaviour of the material. Understanding the thermodynamic and geometric change during annealing of metals has been a subject of interest for a long time. Due to improvement in the electron microscopy techniques, it is possible to map the 2D section of a material using EBSD (Electron Back Scattered Diffraction). This allows one to quantify the geometrical aspects of each grain. For example area, perimeter, misorientation distribution around a grain, number of neighbors, edge distribution, etc. For 3D measurements like volume and surface area, serial sectioning method is used to compile data from multiple 2D layers. There is a mathematical model by Saltykov, using which one can construct a 3D distribution of sizes using the measured 2D distributions. This has been examined on Ni based superalloys but the correlation between experimental results and mathematical prediction is found to be not very satisfactory[4]. In 3D, grain volumes are known to have an exponential distribution and grain areas to have lognormal distribution in self-similar regime. There have been many attempts to model this phenomenon mathematically. Exponential distribution of grain volumes has been derived using a modified Hillert model from the assumption of maximum chaos in grain structure[70]. Triple junctions are nodes where 3 grain boundaries meet. A model based on the disappearance of triple junctions during grain growth is derived by Kinderlehrer et. al.[2] show that the simulation results using this model are also in close correspondence with the experimental observations. Hillert assumed that the velocity of

the grain boundary is proportional to the curvature and the constant of proportionality may be regarded as the mobility of grain boundary. Applying the theory of Ostwald ripening, Hillert found the universal grain size distribution[66]:

$$f(u) = (2e)^{\beta} \frac{\beta u}{(2-u)^{\beta+2}} (e)^{\frac{-2\beta}{(2-u)}},$$

where $u=R/R_{av}$ and $\beta=2$ for 2D and $\beta=3$ for 3D. Here R is the individual grain size and R_{av} is the average grain size.

Behaviour of polycrystals to any addition of energy is a result of evolution of their microstructures, which in turn are a combination of mesoscopic objects like grain boundaries, dislocations, voids, etc. A major conclusion of many experimental[12]-[14] and numerical simulation studies[57],[58] is the existence of a universal grain size distribution. In recent decades, particularly computer simulations have been used to help understand experiments. One of the earliest known approaches is the use of the Monte Carlo Potts model[9],[10], where only the grain boundary faces controls the growth kinetics via their specific energy and mobility. Higher order junctions have no influence on the migration kinetics. This is not the case when the average grain size is small. The volume of triple and quadruple junctions is large enough to not be ignored[11].

Besides, grain boundary dynamics is not governed by just mean curvature flow as it is also affected by impurities, number of grain sides and properties of vertices and grain edges[53]-[55]. A model suggested by Pande (1987) also characterizes each grain by one number, the grain size. However, this approach is different from Hillert's as it contains a fitting parameter just like the widely used log-normal distribution[68]. Analytical solutions

made it possible to observe that the expected features of entropy holds, if one means by entropy the usual Boltzmann entropy. It has been recognized in various branches of material science that thermodynamic description of materials with microstructure requires two additional thermodynamic parameters, entropy of microstructure and temperature of microstructure. Such parameters have been mentioned under different names in theory of granular materials[20]-[22], metal glasses[23]-[37], crystal plasticity[38]-[43], composite materials[44], and grain growth[45]-[48].

ENTROPY DECAY DURING GRAIN GROWTH

It was claimed that there is one more law of thermodynamics: *entropy of microstructure must decay in isolated systems*[49]. One mechanism of this special way of evolution is due to the dissipative nature of mesoscopic dynamics. Dissipative equations possess attractors and trajectories of the system in phase space must fall on the attractor[50]. If entropy of microstructure is associated with the volume of phase space as in classical statistical thermodynamics, then the entropy of microstructure must decay as phase volumes moving to an attractor shrink. A different mechanism of microstructure entropy decay is characteristic for driven dissipative systems such as slow plastic deformation of crystals and polycrystals[51],[52]. There is an ambiguity in the choice of entropy of grain boundary structure. The notion of entropy is multifaceted, and the choice depends on the context in which entropy is used. We aim at a macroscopic description of grain growth when the process is described by a few averaged parameters. In classical thermodynamics, entropy arises inevitably as an unavoidable parameter in constitutive equations. Is the situation in grain growth similar? In principle, to answer this question one must develop an average description of grain structure dynamics. This is a formidable task at the moment. It is enough to mention that, formally speaking, grain boundary is an infinite-dimensional object. Though infinite dimensionality is artificial because grain boundary pieces with sizes that are smaller than the interatomic distance do not carry independent degrees of freedom, and some short wave truncation must be made in grain boundary dynamics, a convincing high-dimensional analysis of grain boundary dynamics does not seem to exist. In this work, we aim to check the entropy decay experimentally. We choose the process of grain

growth as the testing ground. Grain growth is ideally fitted to such experimental study because it can proceed in an isolated setting. This can be seen from the following thought experiment. If a polycrystal is heated enough to allow for grain boundary motion to proceed and then thermally isolated grain growth sets up and does not stop as grain boundary motion heats the crystal. The higher temperature increases grain boundary mobility, and the process does not stop. In actual experiment we employ the isothermal setting assuming that the results are similar. We distinguish the total entropy of the grain boundary microstructure $\mathbb{S}_m$ and entropy per one grain S_m^*,

$$\mathbb{S}_m = NS_m^*. \tag{7}$$

Here index *m* stands for microstructure, *N* being the number of grains. Entropy per one grain S_m^* is the Boltzmann entropy.

$$S_m^* = -\int f(v)\, ln\, f(v) v_0 dv, \tag{8}$$

where f(v) is the probability distribution of grain volumes, v_0 some characteristic grain volume.

All parameters in (7) and (8) evolve in the course of grain growth. In the analytical study[47], parameters S_m^* and $\mathbb{S}_m$ change in opposite directions: entropy per grain S_m^* increases, while total entropy $\mathbb{S}_m$ decays. Increase in S_m^* indicates the chaos enhancement while the decay of $\mathbb{S}_m$ corresponds to the general concept of entropy decay in closed systems. Besides, there is an equation of state: entropy is a function of total energy of grain boundaries $\mathrm{E_m}$ and average grain volume v,

$$\mathbb{S}_m = \mathbb{S}_m(E_m, v). \tag{9}$$

In the work reported here, we study the evolution of S_m^* and $\mathbb{S}_m$, and the validity of the equation of state (9). Briefly, the results are as follows: total entropy $\mathbb{S}_m$, decays as expected, entropy per one degree of freedom S_m^* fluctuates slightly not showing a certain trend, while the equation of state (9) degenerates into equation of the form $\mathbb{S}_m = \mathbb{S}_m(E_m)$.

To find entropy from these experiments one must specify a finite-dimensional version of (8). As such we use the relation,

$$S_m^* = -\sum p_i \ln p_i. \tag{10}$$

Probabilities p_i in (10) are interpreted in the following way: the possible values of grain sizes are split in bins and p_i is the portion of grains in the i^{th} bin. In such interpretation, the values of S_m^* depend on the bin size. To minimize the bin size dependence, we average S_m^* over various values of bin sizes. Note that both S_m^* and $\mathbb{S}_m$ are dimensionless. It is assumed also that in cross-sectional measurments of cross-sectional grain area and cross-sectional grain perimeter correspond to grain volume and grain area of 3D theory, respectively. So, in formula (10) p_i are probabilities of observing certain values of cross-sectional grain area.

According to (7), the evolution of total entropy $\mathbb{S}_m$ is determined by the competition of the decay rate of the number of grains and the rate of increase of S_m^*. In the analytical

study[47], grains disappear at a faster rate than the growth rate of S_m^*, resulting in the decay of total entropy $\mathbb{S}_m$. The experimental values of S_m^* are presented in fig. 1.

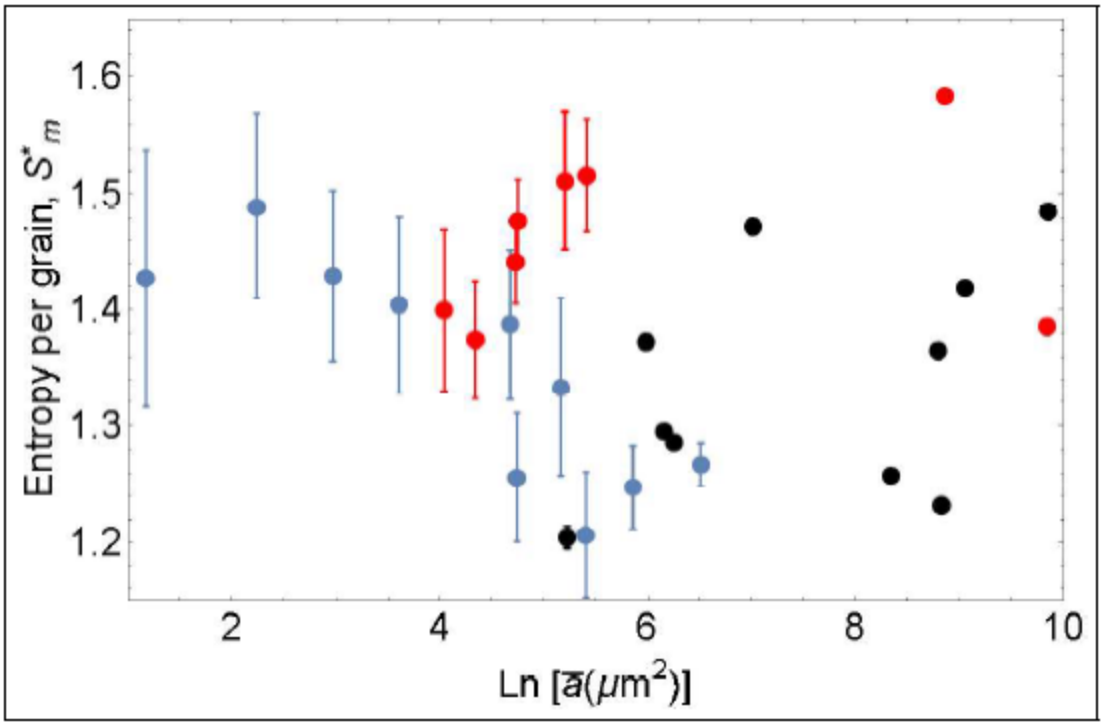

Fig. 1. Evolution of entropy per grain S_m^* as a function of logarithm of mean area $\bar{a}$(μm²). The black and red dots correspond to commercially pure nickel and aluminum alloy Al5083F[71], respectively. Blue dots show the values computed from the data by Bhattacharya et. al.[72] for magnesium alloy AZ31bMg. Error bars are also shown. For larger grain sizes, the error bars are smaller than the displayed points.

It appears that S_m^* does not exhibit a certain trend fluctuating slightly over the average value of 1.4. Thus, the decay of number of the grains N yields the decay of total entropy $\mathbb{S}_m$. The evolution of entropy per unit volume $S_m = \mathbb{S}_m/|V|$ in grain growth is shown in fig. 2. Most likely, small variations of S_m^* are due to the fact that all samples tested have

the initial grain size distribution which is very close to self-similar distribution, and the evolution proceeds along the self-similar path.

In general, S_m is expected to be a function of energy per unit volume and grain size. For definiteness, we take as a characteristic of grain size the average grain volume v. Since energy per unit volume can be assumed to be proportional to average grain 3D surface area a, entropy per unit volume S_m can be considered a function of a and v, $S_m = S_m(a, v)$. Presumably, there is a link between a and v and cross-sectional characteristics of grain geometry, $\bar{a}$ and $\bar{p}$, which allows one to consider S_m as a function of $\bar{a}$, $\bar{p}$. Area and perimeter are independent geometric parameters of grain cross-sections, and making measurements of $\bar{a}$, $\bar{p}$ and S_m we expected to get a set of points in $(\bar{a}, \bar{p}, S_m)$-space, which would yield the equation of state $S_m = S_m(\bar{p}, \bar{a})$. Surprisingly, for all microstructures at all temperatures considered the points collapse on a line shown in fig. 2 indicating an independence of S_m on $\bar{a}$.

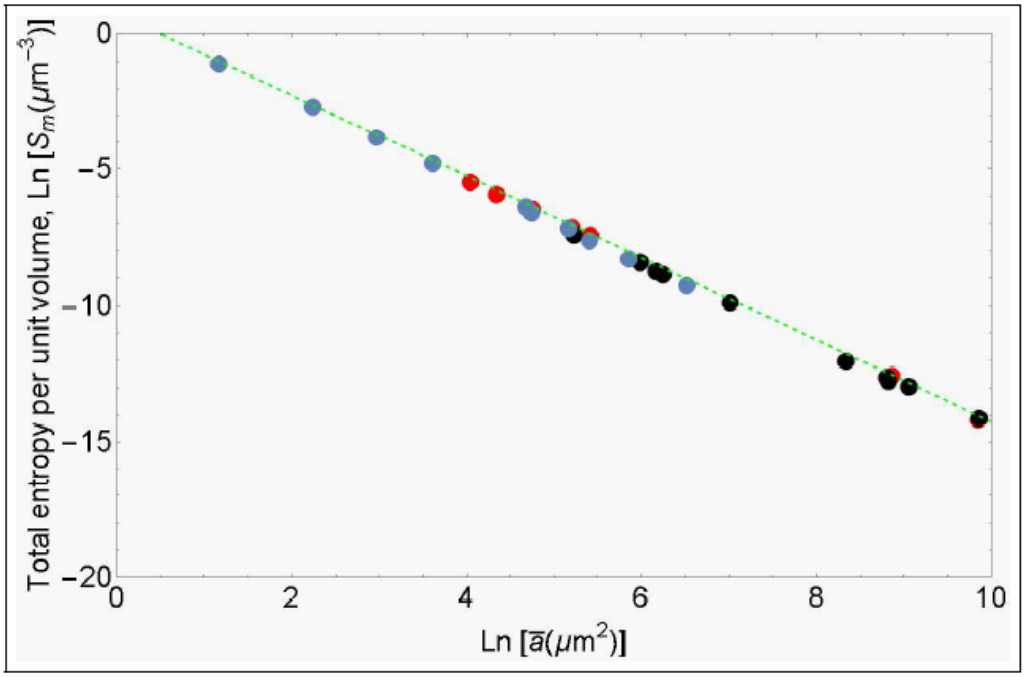

Fig. 2. Dependence of logarithm of entropy per unit volume S_m on logarithm of mean cross-sectional grain area $\bar{a}$. S_m and $\bar{a}$ are measured in $\mu m^{-3}$and μm^2, respectively. The black and red dots correspond to commercially pure nickel and aluminum alloy Al5083F[71], respectively. Blue dots show the values computed from the data by Bhattacharya et al.[72] for magnesium alloy AZ31bMg.

The origin of such degeneration of the equation of state for S_m turns out to be the existence of universal relation between $\bar{a}$ and $\bar{p}$. It is shown in figures below. Emphasize that the points in this figure correspond to annealed microstructures obtained in a wide range of annealing times (1 min-7 days) and annealing temperatures (300°C-1100°C). Fig. 3-5 shows the individual material plots and fig. 6 shows the combined plot for area-perimeter relationship observed in all the grain growth experiments conducted for this study.

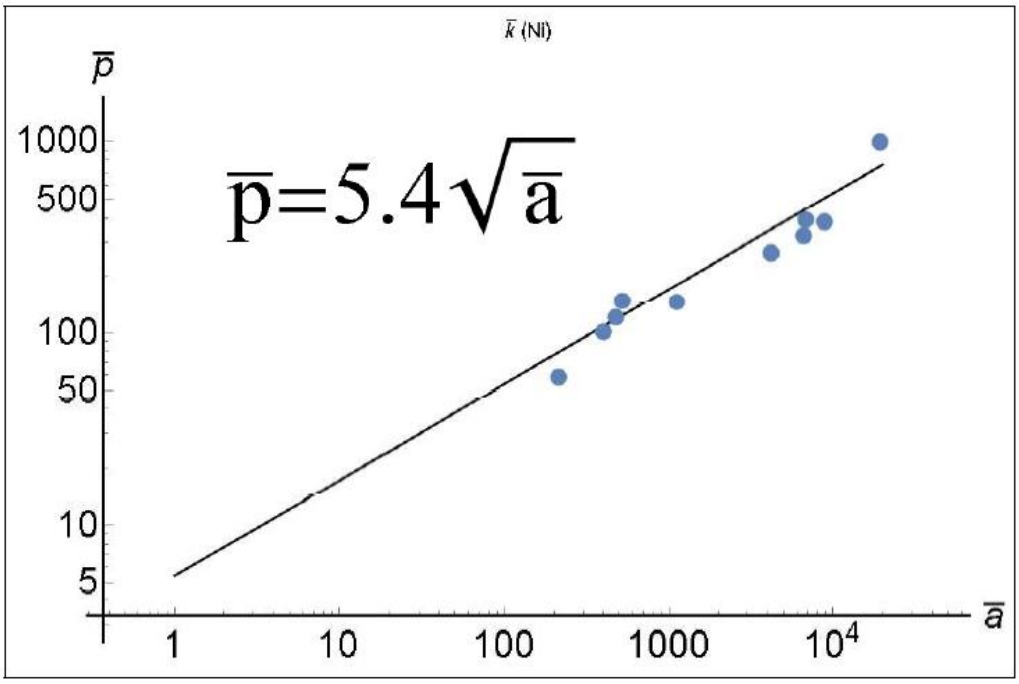

Fig. 3. Relationship between logarithm of mean cross-sectional grain area $\bar{a}$ and logarithm of mean cross-sectional grain perimeter $\bar{p}$ for commercially pure nickel.

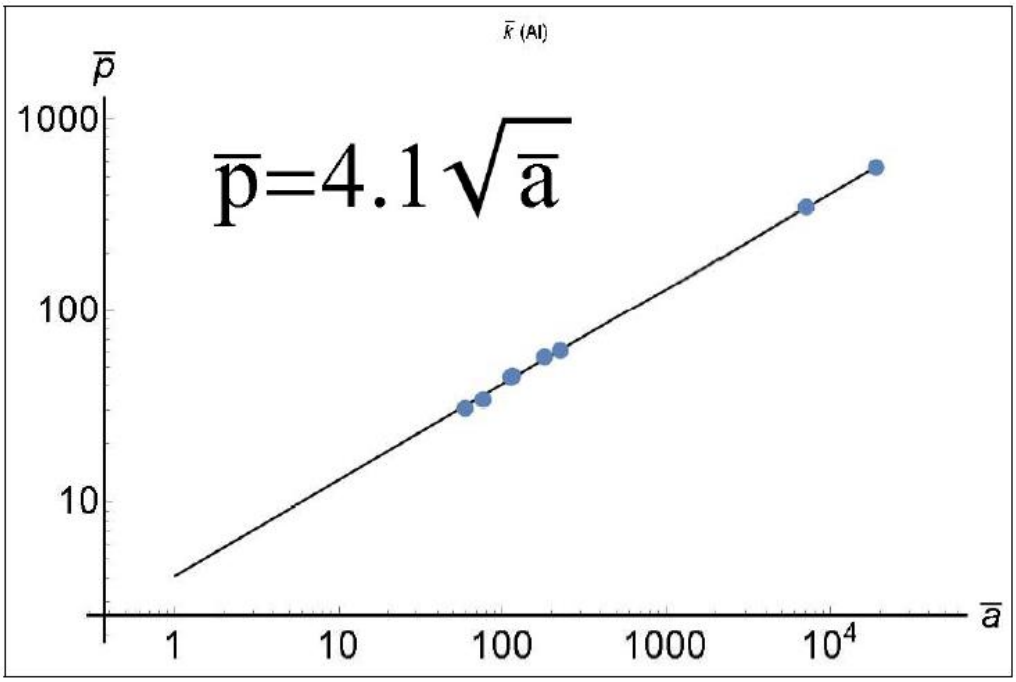

Fig. 4. Relationship between logarithm of mean cross-sectional grain area $\bar{a}$ and logarithm of mean cross-sectional grain perimeter $\bar{p}$ for aluminum alloy Al5083F[71].

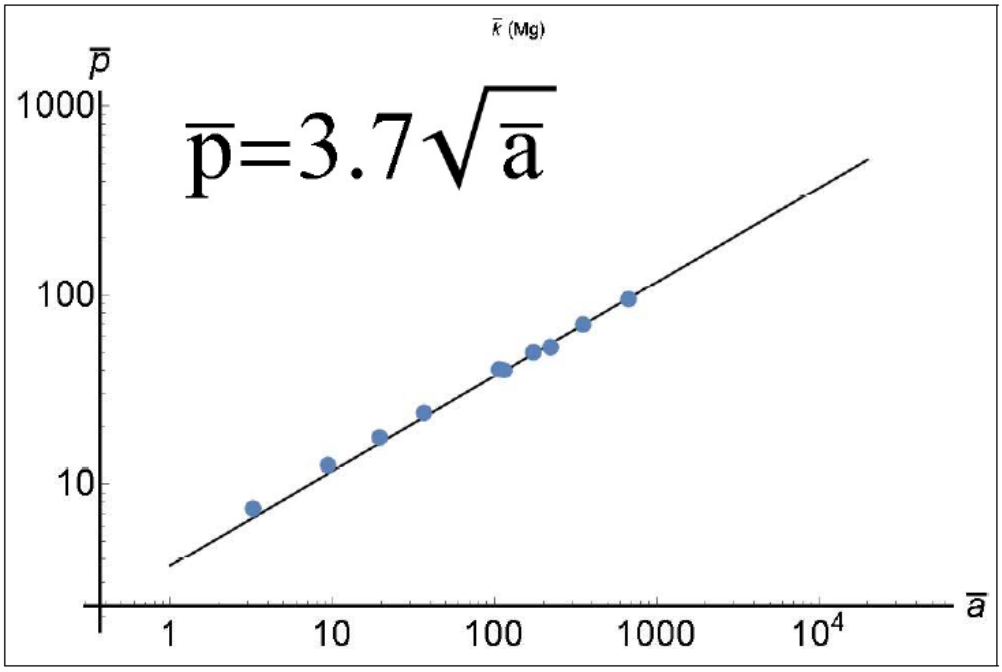

Fig. 5. Relationship between logarithm of mean cross-sectional grain area area $\bar{a}$ and logarithm of mean cross-sectional grain perimeter $\bar{p}$ for magnesium alloy AZ31bMg[72].

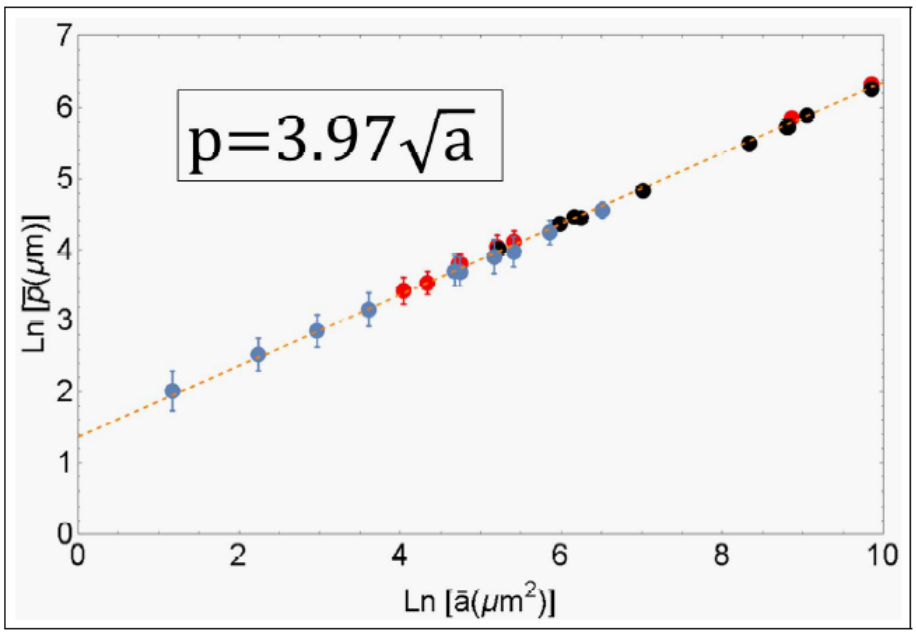

Fig. 6. Relationship between logarithm of mean cross-sectional grain area $\bar{a}$ and logarithm of mean cross-sectional grain perimeter $\bar{p}$. The black and red dots correspond to commercially pure nickel and aluminum alloy Al5083F[71], respectively. Blue dots show the values computed from the data by Bhattacharya et al.[72] for magnesium alloy AZ31bMg.

The relation between mean cross-sectional grain perimeter and mean cross-sectional grain area can be written as

$$\bar{p} = (3.97 \pm 0.04)\sqrt{\bar{a}}. \quad (11)$$

There was a suspicion that the universality of relation (11) was caused by a special equiaxed geometry of grain structures considered. In order to check that we measured a "form factor" which is introduced for i^{th} grain as the ratios, $k_i = p_i/\sqrt{a_i}$, p_i and a_i being perimeter and area of the i^{th} grain cross-section (in 2D geometry, k_i^2 is referred to as isoperimetric quotient[73]). The observed values of form factors k_i are shown in fig. 7 by dots. Thick dots correspond to averaged values of form factor k, K.

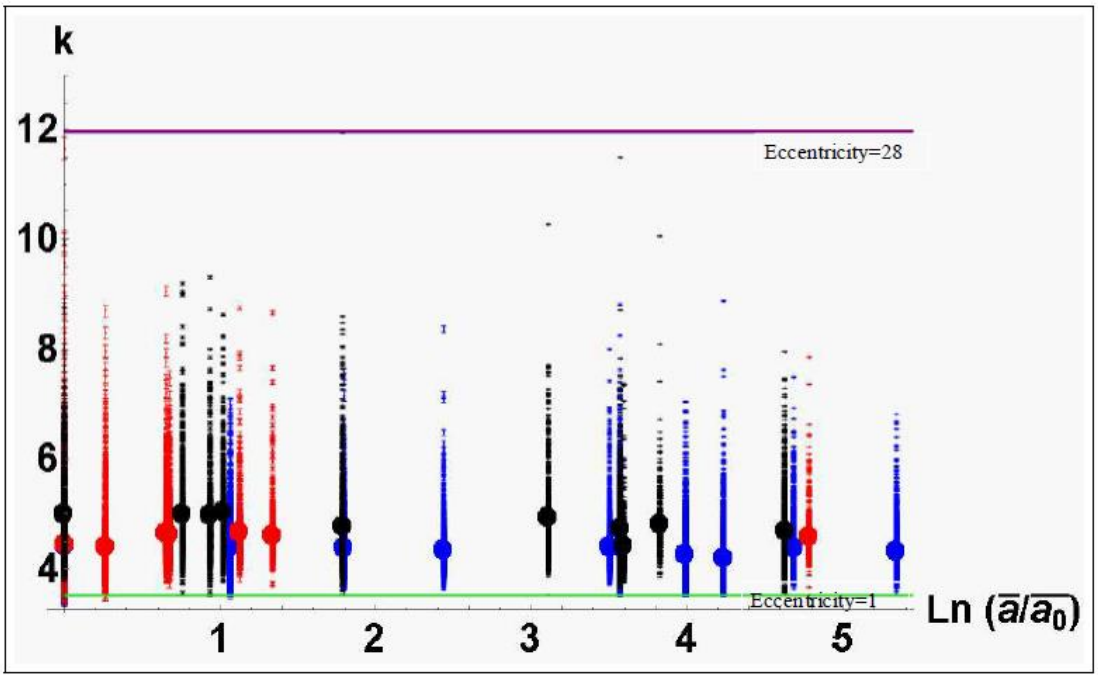

Fig. 7. Experimental values of form factor k for various stages of grain growth shown in terms of mean area $\bar{a}$ normalized by as-received sample's mean area $\bar{a}_0$. The black and red dots correspond to commercially pure nickel and aluminum alloy Al5083F[71] respectively. Blue dots show the values computed from the data by Bhattacharya et al.[72] for magnesium alloy AZ31bMg. Two horizontal lines show the values of eccentricity for circular cross-section (green line, k=3.54, eccentricity 1) and grains with maximum observed eccentricity (purple line, k=12, eccentricity 28).

Since grains do not have wiggly boundaries, parameter k can serve as a measure of grain eccentricity. If the grain cross-section is an ellipse with semi-axes b and c, c≥b, then

$$k = bE(1 - e^2). \tag{12}$$

where $e=c/b$ is eccentricity, and $E(x)$ is complete elliptic integral of second kind. From the measured values of k_i, one can find the corresponding eccentricity. Two horizontal lines in fig. 7 correspond to eccentricity equal to 1 (circle) and the maximum measured

value of k corresponding to eccentricity 28. Note that fig. 7 shows the grain shapes vary quite noticeably in the data presented in fig. 6.

In metallurgy, the mean grain size R is usually determined by measuring the number of grains N in a given volume V . Then R is defined as $(3V/4\pi N)^{1/3}$ or, in terms of average grain volume v, $R = (3v/4\pi)^{1/3}$; v and R are two interchangeable characteristics of grain size. Energy of the grain structure is proportional to average grain areas. In order to determine the dependence of energy on grain size, one must find a link between average 3D grain area a and average grain volume v. Fig. 6 suggests that there might be a relationship similar to (11),

$$v = \alpha a^{\frac{3}{2}}. \tag{13}$$

As for cross-sectional geometry, 3D parameters of grain structure a and v are statistically independent, and the very fact that formula (13) holds true needs an experimental verification. No experimental results supporting the validity of (13) seem to exist, though there are various assumptions on the character of randomness of grain topology[74]-[81]. Our estimation of α is α~0.1. The calculation is provided in appendix C.

If relation (13) holds true indeed, then entropy degenerates, and S_m becomes a function of either a or v. Let us take for definiteness $S_m = S_m(v)$. If one can use in 3D the values of S_m^* found from cross-sectional measurements, $S_m^* \sim 1.4$.

$$S_m = 1.4v^{-1}. \tag{14}$$

or, in terms of a

$$S_m = 1.4\alpha^{-1}a^{-3/2}.$$

On the other hand, grain boundary energy per unit volume, $U_m = E_m/V$, is

$$U_m = \frac{\Upsilon a}{v} = \frac{\Upsilon \alpha}{\sqrt{a}}. \tag{15}$$

Υ being grain boundary energy per unit area. Relations (14) and (15) yield the equation of state

$$U_m = \beta S_m^{1/3} \tag{16}$$

where the parameter β is $\Upsilon(1.4\alpha^2)^{-1/3}$.

MATERIALS AND EXPERIMENTAL METHODS

A. MATERIALS

A.1 Nickel microstructure analysis

The nickel samples were cut 10-12mm each from commercially pure 0.25" rod (from McMaster Carr). The annealing of samples was done in closed furnace for all the samples for different temperatures and times.

Table 1. Temperatures and times of annealing for Ni samples

Temperature ($°C$)	Time (min)		
850	5	30	240
1000	5	30	180
1100	5	30	90

The sample was put in the OTF-1200X furnace (manufactured by MTI Corporation) roughly 100°C before it reached the required annealing temperature. Once the annealing time was complete, sample was removed, and air cooled to bring it back to room temperature. Each sample was then hot mounted using epoxy. The mounted samples were then prepared for EBSD by hand polishing. The following Si-C grit papers were used: 180, 320, 600, 1200. Cloth polishing was done with 5 different sizes of diamond paste. The final polishing was done using colloidal silica solution on a silk cloth and the time required for each sample was between 30 mins to 1 hour for this step. Post-polishing, the samples were cleaned using an ultrasonic cleaner to make sure no residual dust particles exist.

EBSD of each sample was done as close to the center as possible in order to avoid the edges and free surface. The instrument used for EBSD is JSM 7600 FE SEM. The voltage of SEM was set at 20kV for all the scans. Multiple scans were done on different areas of the sample to make sure that we have at least 300-350 grains for each of the conditions. The step size varies from 2 um for as received to 15 μm for the samples heated at high temperature for longer time. After getting the EBSD scans through OIM data collection software, they were analyzed and all points with CI < 0.1 were removed. Grain dilation method was used for getting the final cleaned image for each scan. All the grains were then hand-traced using Image-J software to get the statistical information about the area and perimeter. The error in the measurement is calculated from the minimum area and perimeter measurable by the software which is usually 1-4 pixels of the image. All the microstructure images are shown in appendix B.

A.2 Magnesium microstructure analysis

The detailed method of getting the magnesium microstructure images has been explained in [72]. Optical microscope image of surface of annealed samples after etching are shown in appendix B. The grain boundaries which are visible in the images were hand-traced and the area near the edges was avoided to gather data from the grains which are completely captured in the image.

Table 2. Temperatures and times of annealing for AZ31bMg samples

Temperature ($°C$)	Time (min)		
300	4	4320	10080
400	4	60	1080
450	1	4	1320

A.3 Aluminum microstructure analysis

Al 5083F is a fine-grained aluminum alloy developed by Alcoa for superplastic forming and the grain growth data for this material was provided by Dr. Huibin Wu[71]. The post polishing EBSD microstructure images (example shown in appendix B) were also processed the same way as the nickel samples (by hand tracing).

Table 3. Temperatures and times of annealing for Al5083F samples

Temperature ($°C$)	Time (min)	
450	-	60
500	60	180
550	60	180
600	60	300

B. METHODS

B.1 Microstructure cross-section topology

Once the microstructure image is obtained, grain boundaries were hand traced. All the lighter components of the image were thresholded in order to highlight the skeleton of traced grain boundary network. Appendix D shows examples of images before and after grain boundary tracing. Sources of error in measurement of cross-sectional area and perimeter: There are systematic errors which inherently exist when carrying out the analysis of the traced grain boundary images. Image-J has an adjustable parameter (a_m) specifying minimum measurable area. Range of a_m is 0.25 μm² to 10 μm² depending on the value of mean cross-sectional area of the microstructure. As a_m is specified manually, this leads to the software ignoring grains smaller than a_m. This leads to overestimation of mean 2D characteristics of grain structure. Tracing of grain boundaries was done with a brush of fixed width (2 pixels) which is the source of error in perimeter measurement. p_m, minimum measureable perimeter will be of the order of width of traced grain boundaries. Range of p_m is 0.5 μm to 2 μm. Error in measurement of cross-sectional area and perimeter of grains propogates further in the calculation of entropy per grain S_m^* and microstructure entropy per unit volume S_m.

$$Err_a = \frac{a_m}{\bar{a}}, Err_p = \frac{p_m}{\bar{p}}. \quad (17)$$

where Err_a and Err_p are measurement errors in cross-section area and perimeter. The overall effect of these errors is significant on the microstructure images with smaller average grain size. We get less than 2% error as grain growth proceeds.

B.2 Calculation of 2D characteristics

The cross-sectional area and perimeter of each grain are known. This allows one to calculate the mean value of the 2D parameters using formula shown below.

$$\bar{a} = \frac{a_1 + \ldots + a_N}{N}, \bar{p} = \frac{p_1 + \ldots + p_N}{N}. \quad (18)$$

where $\bar{a}$ and $\bar{p}$ are mean cross-sectional area and perimeter, respectively, a_i is the 2D cross-sectional area of i^{th} grain, p_i is the 2D cross-sectional perimeter of i^{th} grain and N is the total number of grains measured in the section. Additional characteristics of the microstructure can be determined from the measurement of cross-sectional area and perimeter of each grain. A dimensionless form factor, k_i has been introduced for i^{th} grain. Note that this k_i is different in definition from k used in the previous chapter. Mean value of measured k_i for a given microstructure denoted by K is also calculated (shown in fig. as large dots). Another parameter $\bar{k}$ is calculated using the following relation

$$\bar{k} = \bar{p}/\sqrt{\bar{a}}. \quad (19)$$

where $\bar{a}$ and $\bar{p}$ are known mean cross-sectional area and perimeter, respectively.

B.3 Grain size distribution

Volume of the grain is estimated based on the assumption that grains are spherical. This may not always be the case, but it has been proven to be a convenient approximation. The equivalent circle diameter d_a and equivalent sphere diameter d_s are calculated using equation shown.

$$d_a = \sqrt{\frac{4a_i}{\pi}} = \frac{\pi}{4} d_s. \tag{20}$$

The volume of individual grain v_i will then be given by

$$v_i = \frac{\pi}{4} {d_s}^3. \tag{21}$$

The next step of the analysis is to get the grain size (normalized volume) distribution of the microstructure. Average volume of the microstructure $\bar{v}$ is calculated in the same way as cross-sectional area and perimeter shown in (18). Each grain volume, v_i is normalized by average volume giving one dimensionless number $v_i/\bar{v}$ to characterize a grain. From (20) and (21), one can observe that normalized volume and normalized area are linked as

$$\frac{v_i}{\bar{v}} = \left(\frac{a_i}{\bar{a}}\right)^{\frac{3}{2}}. \tag{22}$$

Normalized volume of all the grains is then divided into bins to count the total number of grains within that bin. The probability of finding a grain in a particular bin is the ratio of number of grains in the said bin to the total number of grains. After getting grain size distribution, entropy per grain is calculated. Fig. 8 shows example of grain size distribution for different metals and their respective stages of annealing. The initial and

final volume distribution of all the chosen materials is far from self-similar as the microstructure is evolving towards a steady-state.

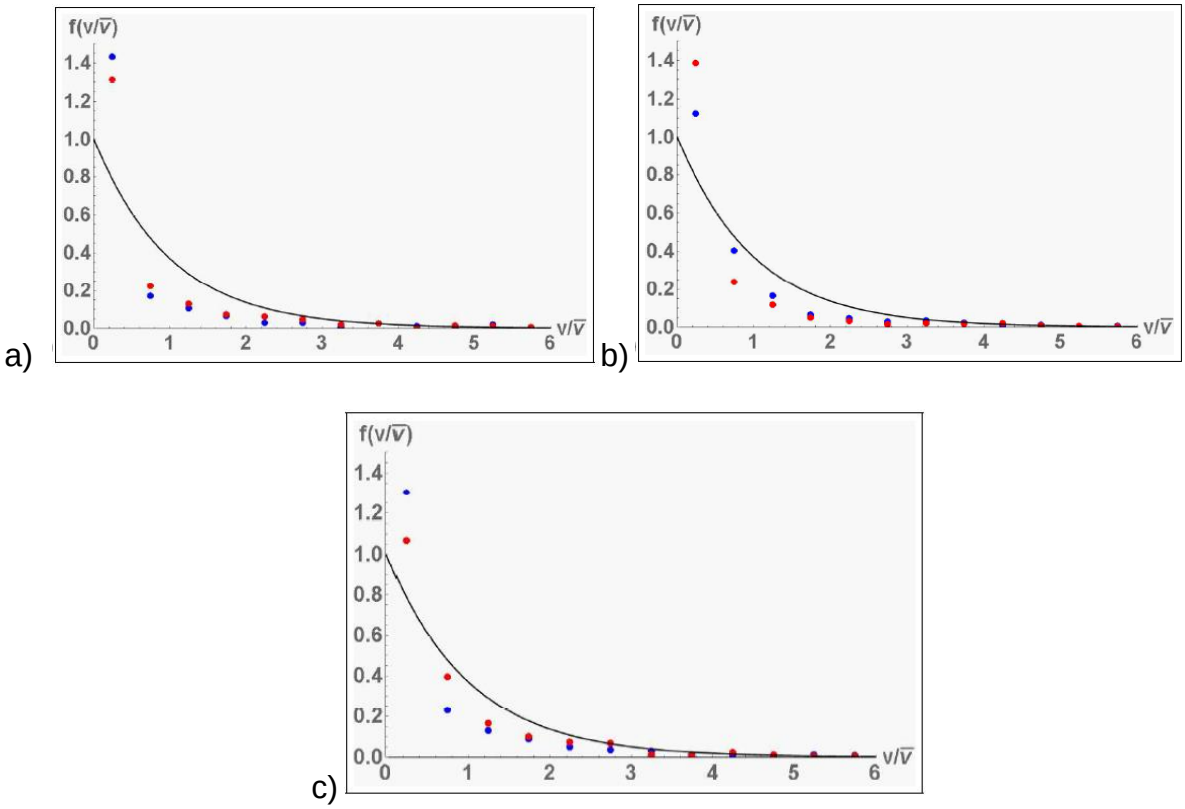

Fig. 8. a) Grain size (normalized volume) distribution for as-rec (blue dots) and sample annealed at 1000°C for 180min (red dots) nickel samples, b) Grain size (normalized volume) distribution for as-rec (blue dots) and sample annealed at 450°C for 22hr (red dots) AZ31bMg samples, c) Grain size (normalized volume) probability distribution for as-rec (blue dots) and sample annealed at 600°C for 1hr (red dots) Al5083F samples. The black curve is exponential distribution which corresponds to self-similar grain growth[70]. The bin size used here is 0.5.

B.4 Calculation of entropy per grain, S_m^*

Entropy per grain for a given microstructure is calculated from the definition of S_m^* as given by (10). The value of entropy per grain S_m^* is dependent on selected bin size. The reasoning is that the value of probability of finding a particular grain size is dependent

on the bin size chosen hence affecting the final size distribution (example shown in fig. 9a) qualitatively. Fig. 9b shows how S_m^* depends on bin size.

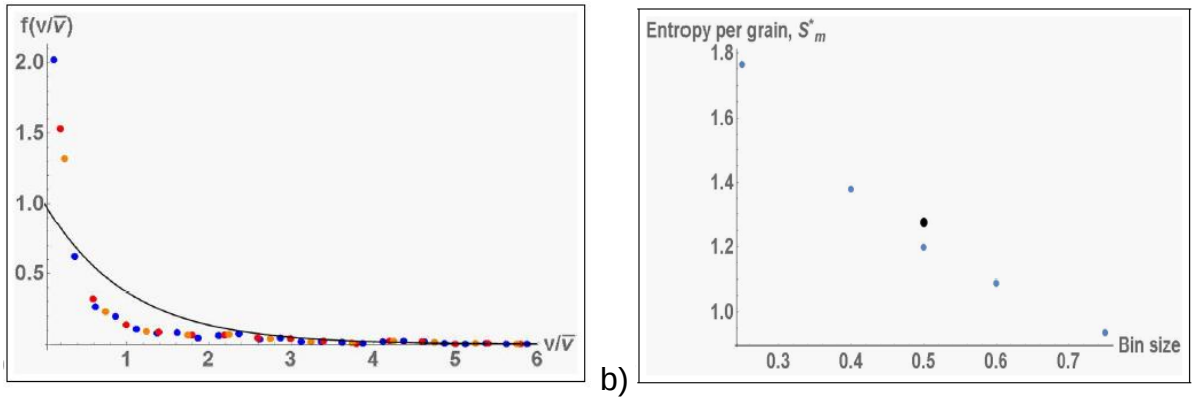

Fig. 9. a)Volume probability distribution of annealed (Temp.- 850°C,time - 240 min) nickel sample. S_m^* values are 1.8, 1.4 and 1.2 for bin sizes 0.25 (blue dots), 0.4 (red dots) and 0.5 (orange dots), respectively. b) Dependence of S_m^* on bin sizes for the same sample. The black dot is average value of S_m^* over the selected range of bin sizes.

To make S_m^* invariant to bin size, the following method is applied: Entropy per grain S_m^* for each individual sample is found out by taking an average over a range of bin sizes. The bins chosen for this study are 0.25, 0.4, 0.5, 0.6 and 0.75. This leads to a simplification in calculation of S_m^*.

$$S_m^* = -\sum_i \frac{n_i}{N} ln \frac{n_i}{N} \tag{23}$$

Here n_i is the count of grains in i^{th} bin and N is the total number of grains considered. Microstructure entropy per unit volume is estimated $v_i/\bar{v}$ as,

$$S_m = S_m^*/\bar{v} \tag{24}$$

NEW STATISTICAL PARAMETERS FOR GRAIN GROWTH

Grain boundary surface being of arbitrary shape has infinite degrees of freedom. This makes the choice of proper finite-dimensional truncation a quite non-elementary issue. Some finite-dimensional models have been discussed in ([56]-[64]). Here we will employ the crudest dynamic model possible: it presents the grain boundary structure as a "gas of grains", where each grain is characterized by one number, either grain volume or grain radius. This starting point of the model was explained in an unpublished work by Berdichevsky[65]. The complete treatment and the equations derived is presented in what follows. Grains can grow and shrink and do not have "energetic" interactions, i.e. the total energy of the grain structure is the sum of energies of individual grains with the factor 1/2 as each piece of grain boundary provides the same contribution to energies of two neighboring grains. The interaction of grains arises from the kinematic constraint: the sum of volumes of all grains is preserved. This model goes back to the work by Hillert[66], and was further developed in many studies[67]-[70]. Hillert obtained an equation for probability distribution of grain sizes which is mentioned earlier. This equation was modified by Berdichevsky[47] to allow for analytical solutions.

During grain growth, an initially random structure achieves a steady state by dissipating energy. This dissipative system and related thermodynamics is studied using a modified Hillert type approach. It is observed that the microstructure entropy decays as self-similar regime is achieved[47]. The study of grain growth in nano-scale thickness films (thin films) of aluminum and copper show that there exists a universal experimental grain size distribution[83].

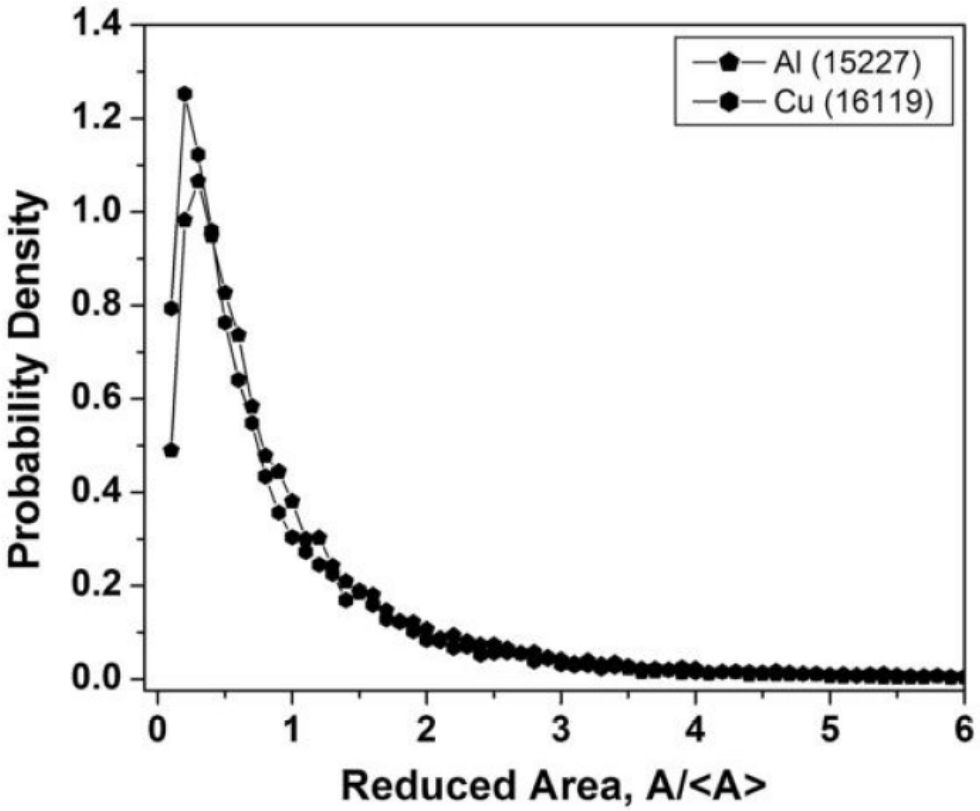

Fig. 10. Universal grain size distribution in Al and Cu thin films[83]. x-axis is the dimensionless grain size was calculated by normalizing the actual area by mean area of the grain structure.

As seen in the fig. 10 above, the grain size distribution is very different from the exponential grain size distribution in micro-scale thickness films. The shape of the probability distribution of reduced grain areas equation is very similar to the grain size distribution of pure nano thickness films, hence this can also be applied to thin films.

In this work, from the maximum chaos hypothesis a probability distribution of grain sizes is derived which uses two new statistical characteristics of grain microstructure, k and $\varkappa$. One takes into account the individual non circularity of the grains namely, k and the other defines the combined statistics of all grains in the microstructure by virtue of the mean area and mean perimeter of the microstructure, $\varkappa$. Measuring these

characteristics from a given microstructure, one can construct probability distribution of areas and perimeters of grains. The grain size distributions in AZ31b magnesium alloy are compared with the derived equations. We find that the equations describe the experimentally observed data reasonably well. Usually the probability distribution obtained develops after some annealing and may not be observed in as received microstructures. An example fit is shown in fig. 11.

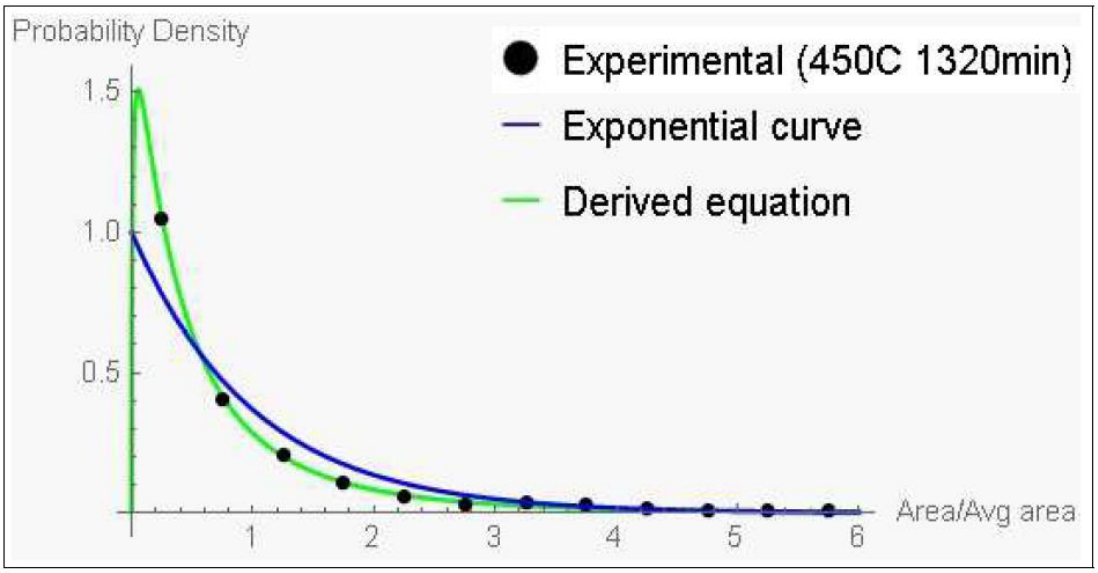

Fig. 11. Black dots - Experimental data points for AZ31b annealed at 450°C for 1320 mins[72]. Blue line - $f(a/\bar{a}) = e^{-(a/\bar{a})}$. Green line -Equation (31) with characteristics derived in this model (k =0.288, $\varkappa$ =1.062)

The evolution of the proposed characteristics has also been studied by varying the annealing time and temperature. In this chapter an alternative statistical model has been suggested for 2D distribution of relative grain areas and perimeters. We describe each grain by two number, area of the grain, ‘a' and the perimeter of the grain, ‘p'. So, the grain dynamics of N grains is considered in a 2N dimensional space of parameters, $a_1,\ldots, a_N, p_1,\ldots, p_N$. According to isoperimetric inequality, only part of phase space is

admissible for phase flow: $a_1 \leq ((p_1)^2/(4\pi)), \ldots, a_N \leq ((p_N)^2/(4\pi))$. The isoperimetric inequality bounds a_i from above by p_i. In real polycrystals grains do not have arbitrary shapes and one cannot bound a_i from below by p_i. We have introduced a positive constant by means of which all a_i can be bounded from below. We define a new parameter, k

$$k = \min_i \frac{4\pi a}{p^2}. \tag{25}$$

k =1 would mean that the grain is a perfect circle in shape whereas very small values of k would mean elongated grains. k always lies between 0 and 1. Total perimeter is calculated as

$$P = \frac{1}{2}\sum_i^N p_i. \tag{26}$$

Total area is given by,

$$A = \sum_i^N a_i. \tag{27}$$

Total energy, E is considered to be a function of the perimeter of each grain and a constant γ, energy per unit length of grain boundary.

$$E = \frac{\Upsilon}{2}\sum_i^N p_i. \tag{28}$$

A factor of $(1/2)$ is introduced as perimeters are counted twice when added for all the grains present.

We make the following basic assumptions:

1. Tessellation condition holds[47]. It simply addresses the fact that all grains cannot be circular to fill the microstructure with no gaps.

2. In the course of grain dynamics, some non-zero value of k such that 0≤k, is developed.

3. All admissible values of (a,p) are equiprobable.

Under these assumptions, the statistics of grain areas and perimeters is investigated. The resulting equations are not simple enough to be completely solved analytically. We have used Wolfram Mathematica 10 for all the plots used in this thesis. The code used is shown in Appendix C.

We introduce another parameter $\varkappa$ for simplification of solution, which is defined as

$$\varkappa = \frac{\bar{p}^2}{4\pi\bar{a}}. \tag{29}$$

In particular, we obtain two distributions for relative perimeters, $\frac{p}{\bar{p}}$ and areas, $\frac{a}{\bar{a}}$ as follows

$$f\left(\frac{p}{\bar{p}}\right) = c_1 e^{-\check{z}\frac{p}{\bar{p}}}\left[e^{-\check{\zeta}\varkappa \mathrm{k}\left(\frac{p}{\bar{p}}\right)^2} - e^{-\check{\zeta}\varkappa\left(\frac{p}{\bar{p}}\right)^2}\right]. \tag{30}$$

$$f\left(\frac{a}{\bar{a}}\right) = c_1 e^{-\check{\zeta}\frac{a}{\bar{a}}}\left[e^{-\check{z}\sqrt{\varkappa\frac{a}{\bar{a}}}} - e^{-\check{z}\sqrt{\frac{\varkappa a}{k\bar{a}}}}\right]. \tag{31}$$

where c_1 and c_2 are normalizing constants. The detailed derivation of equations (30) and (31) are given in appendix A.

The grain size distribution equations derived in this work, can be applied to any microstructure irrespective of how much strain has been induced and up to what temperature it has been annealed. The history of deformation on the microstructure does not affect the measurement of these characteristics. The correlation of derived equation with real experimental data has been shown in appendix B.

DYNAMIC CHARACTERISTICS OF GRAIN GROWTH

The empirical relation:

$$R = Kt^n. \tag{32}$$

is a universally accepted approximation of kinetics of grain growth in polycrystals where R is the average grain size, t is the time of annealing, K is a temperature dependent constant for mobility and surface energy of grain boundary network and n is the grain growth exponent. Based on the curvature flow reasoning, n=0.5 is the ideal value of n if grain boundaries move at a velocity proportional to the grain boundary local curvature solely to reduce the grain boundary surface tension. As it is seen from fig. 12, n=0.5 is only observed experimentally for very high purity metals and close to melting point. There are several explanations presented by various authors for this observation. The factors which influence grain growth exponent are secondary particle drag and pinning (also called Zener drag), triple and quadruple junctions which become immobile due to stabilization, sub-grain rotation and coalescence, etc.

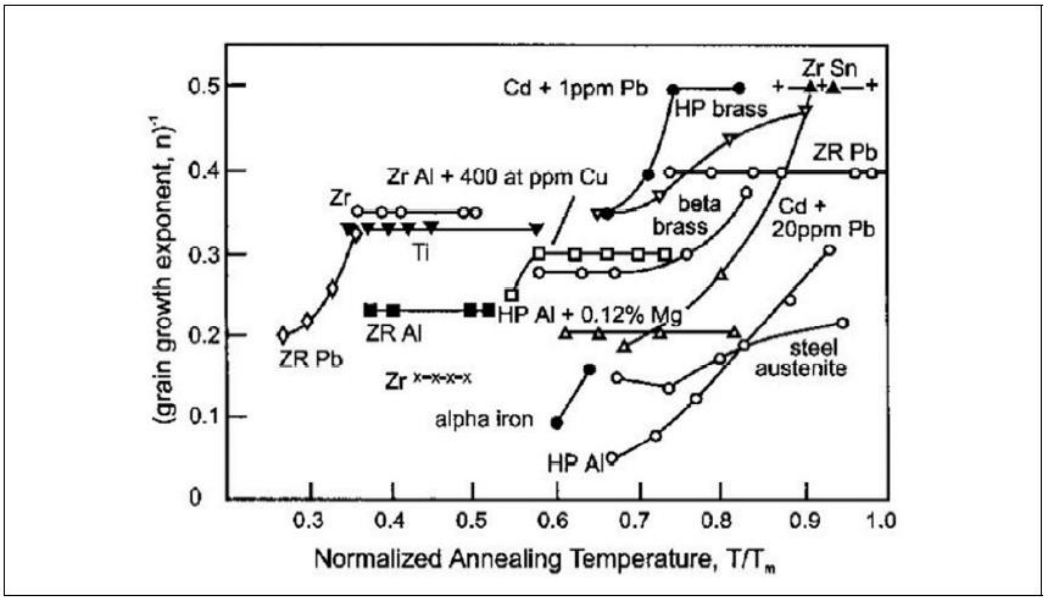

Fig. 12. Temperature dependence of grain growth exponent in a variety of metals[93]. In this plot, the y-axis is inverse of grain growth exponent n shown in eq. (32).

Experimental results obtained in this study have been fit to get the values of K and n. Fig 13-15 shows different temperatures of annealing for Ni, Al and Mg samples, respectively.

a)

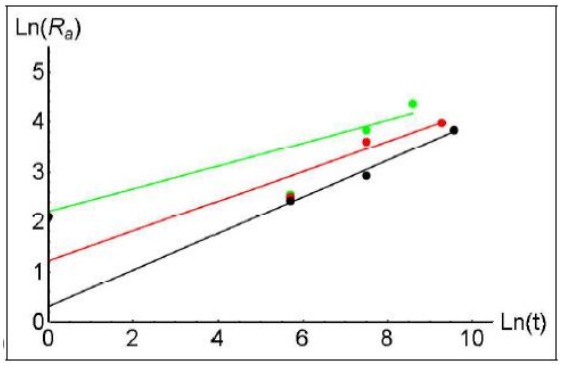

b)

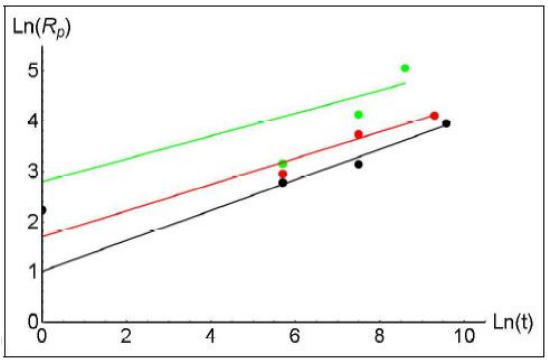

Fig. 13. Grain size as a function of time for Ni samples. a) x-axis is natural logarithm of time in seconds and y-axis is $\sqrt{\bar{a}/\pi}$ which is grain radius as a function of area. b) x-axis is natural logarithm of time in seconds and y-axis is $\bar{p}/2\pi$ which is grain radius as a function of perimeter.

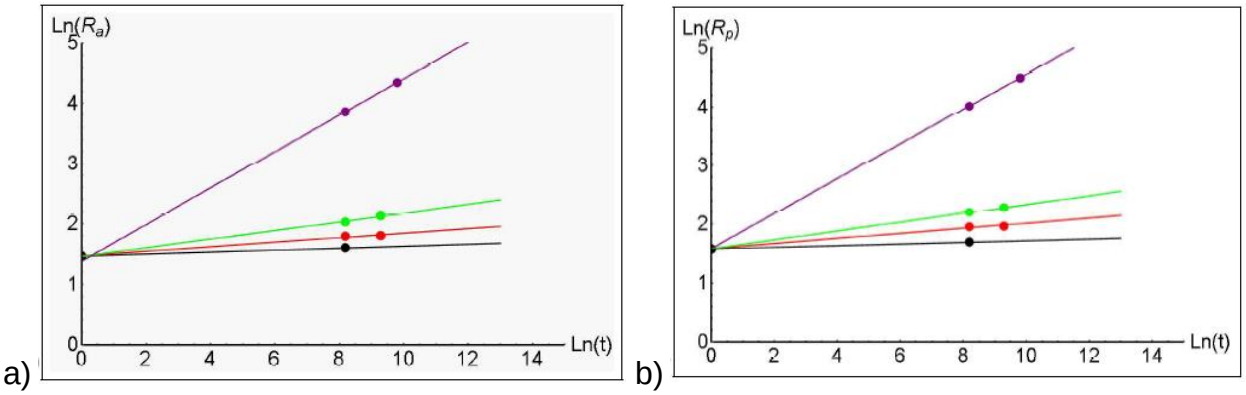

Fig. 14. Grain size as a function of time for Al samples. a) x-axis is natural logarithm of time in seconds and y-axis is $\sqrt{\bar{a}/\pi}$ which is grain radius as a function of area. b) x-axis is natural logarithm of time in seconds and y-axis is $\bar{p}/2\pi$ which is grain radius as a function of perimeter.

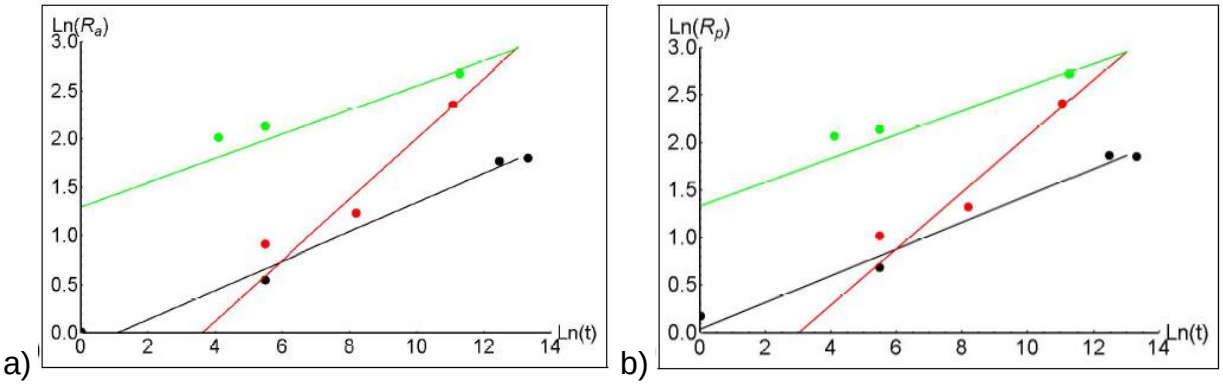

Fig. 15. Grain size as a function of time for Mg samples. a) x-axis is natural logarithm of time in seconds and y-axis is $\sqrt{\bar{a}/\pi}$ which is grain radius as a function of area. b) x-axis is natural logarithm of time in seconds and y-axis is $\bar{p}/2\pi$ which is grain radius as a function of perimeter.

Table 4. Summary of K and n values for all materials and annealing temperatures.

Area data					Perimeter data				
Material	Temp (°C)	K	n		Material	Temp (°C)	K	n	
Ni	850	1.3652	0.3654	Black	Ni	850	2.7581	0.3037	Black
	1000	3.4116	0.2974	Red		1000	5.4642	0.2611	Red
	1100	9.1251	0.2273	Green		1100	16.387	0.2274	Green
Mg	300	0.855	0.1497	Black	Mg	300	1.0379	0.1404	Black
	400	0.3248	0.3127	Red		400	0.4093	0.2959	Red
	450	3.6441	0.126	Green		450	3.7927	0.125	Green
Al	450	4.3292	0.0161	Black	Al	450	4.8739	0.0135	Black
	500	4.3448	0.0375	Red		500	4.899	0.0428	Red
	550	4.3036	0.0715	Green		550	4.8831	0.0749	Green
	600	3.9756	0.3031	Purple		600	4.895	0.2967	Purple

Prediction of final grain size during heat treatment cycles use formula (32) to calculate the expected grain size. However, grain size is an ambiguous term which is usually calculated by considering the equivalent circle radius for the area of a given grain. As seen in chapter 3, perimeter of grain along with grain area is an important characteristic to determine the shape of grains and its overall effect on the microstructure. Table 4 shows that the values of K is different when the radius (or grain size) is calculated using different characteristics, cross-sectional area and cross-sectional perimeter. It can also be observed that the values of K is consistently lower when the radius is calculated from average grain area compared to average grain perimeter. The values of n show an opposite trend. This can be attributed to the finding of equation (11), which indicates that the square root of average 2D cross-sectional grain area and the average 2D cross-sectional grain perimeter linearly correspond with each other.

SUMMARY AND CONCLUSION

The experimental data reported supports the assertion that entropy of microstructure decays in the process of grain growth. Moreover, the equation of state for microstructure entropy per unit volume is degenerated and is given by a simple relation, $S_m = 1.4v^{-1}$. Accordingly, energy and temperature of microstructure are described by the equations of state, $U_m = \beta {S_m}^{1/3}$ and $T_m = \frac{\beta}{3} {S_m}^{-2/3}$.

It is noteworthy that for one-parametric models like the one specified by (16) entropy decay is a consequence of the first and the second laws of thermodynamics. Indeed, according to the first law of thermodynamics, in an isolated system total energy E is conserved. In grain growth, E is a sum of energy of atomic motion, E_{th}, and energy of grain boundaries, E_m. The first law of thermodynamics reads:

$$\frac{dE}{dt} = \frac{dE_{th}}{dt} + \frac{dE_m}{dt} = 0. \tag{33}$$

According to second law of thermodynamics, thermodynamic entropy $\mathbb{S}_{th}$ increases,

$$\frac{dE_{th}}{dt} = T\frac{d\mathbb{S}_{th}}{dt} > 0. \tag{34}$$

In (34) T is the absolute temperature which is defined as $T = dE_{th}/d\mathbb{S}_{th}$. Assuming that microstructure temperature T_m is positive,

$$T_m = \frac{dE_m}{d\mathbb{S}_m} = \frac{dU_m}{dS_m} > 0. \tag{35}$$

We obtain from (33) that microstructure entropy decays,

$$\frac{d\mathbb{S}_m}{dt} = \frac{T}{T_m}\frac{d\mathbb{S}_{th}}{dt} > 0. \tag{36}$$

Note that microstructure entropy decay would not follow from the first and second laws of thermodynamics and would be an independent statement, if microstructure energy E_m was a function of both arguments, v and $\mathbb{S}_m$.

FUTURE WORK

It is likely that the degeneration of constitutive equations is due to the fact that in all the samples tested grain growth followed a self-similar path. In this regard, it would be interesting to study grain growth in materials with bimodal or trimodal initial grain size distribution along with another open question which is to get an experimental verification of relation (13).

APPENDIX A: EVALUATION OF α

Usually grain size is found by linear intercept method in most of the grain measurement experiments. The linear intercept yields the ratio of volume to surface area.

$$P_L = \frac{N_A}{L} = \frac{2}{\pi} L_A, \frac{N_A}{L} = \frac{1}{2} S_V. \tag{37}$$

where P_L is the count of intersections per unit length of line, N_A is the number of intersections, L is the total length of the line intercept drawn, L_A is the ratio of 2D cross-sectional perimeter to area and S_V is ratio of 3D boundary surface area per unit volume. From (37),

$$S_V = \frac{4}{\pi} L_A. \tag{38}$$

In terms of our paper, eq. (38) can be re-written as

$$\frac{a}{v} = \frac{4}{\pi} \frac{\bar{p}}{\bar{a}}. \tag{39}$$

where a, v are 3D average grain area and volume respectively, and $\bar{p}$, $\bar{a}$ are 2D cross-sectional mean perimeter and area respectively. Introducing the definition of "form factor" into eq. (39), α can be found out in terms of the known quantities as

$$\alpha = \frac{0.7}{k^{\frac{3}{2}}} \frac{\bar{a}^{\frac{3}{4}}}{v^{\frac{1}{2}}}. \tag{40}$$

If k=4 is taken as a constant from the experimental data from fig. 3 and fig. 4 of the main text. If the ratio of 2D cross-sectional grain area and 3D volume, $\bar{a}^{\frac{3}{4}}/v^{\frac{1}{2}}$ is considered to be unity, then one gets α~0.1 in (40). For reference, a regular sphere and a regular cube have α=0.095 and α=0.068, respectively. Emphasize, that the relation (38) used for this estimation is based on the assumption which can be interpreted as the ergodicity of space tessellation.

APPENDIX B: Ni EBSD MICROSTRUCTURES AND RELATED DATA

a) 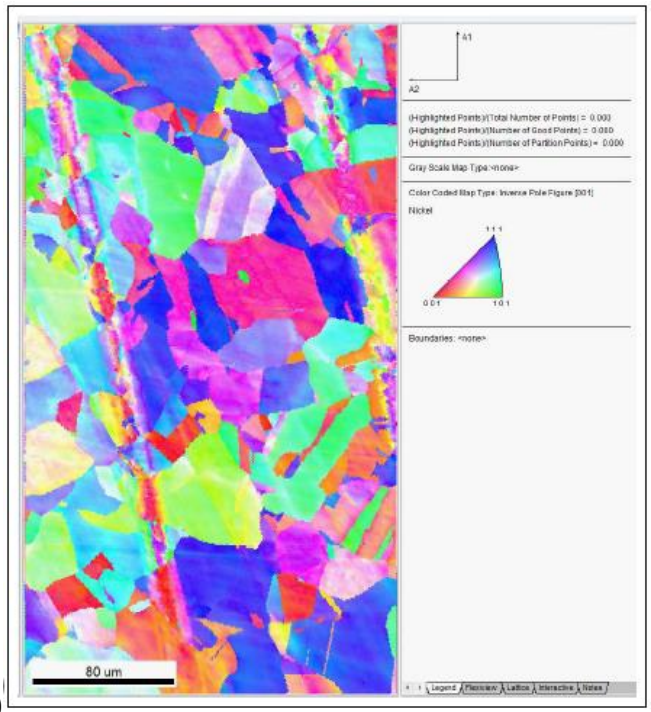

b) 

Figure 16. a) Ni as-received microstructure inverse pole figure, b) Ni as-received microstructure inverse pole figure. The same IPF legend applies to all the other EBSD images in this section

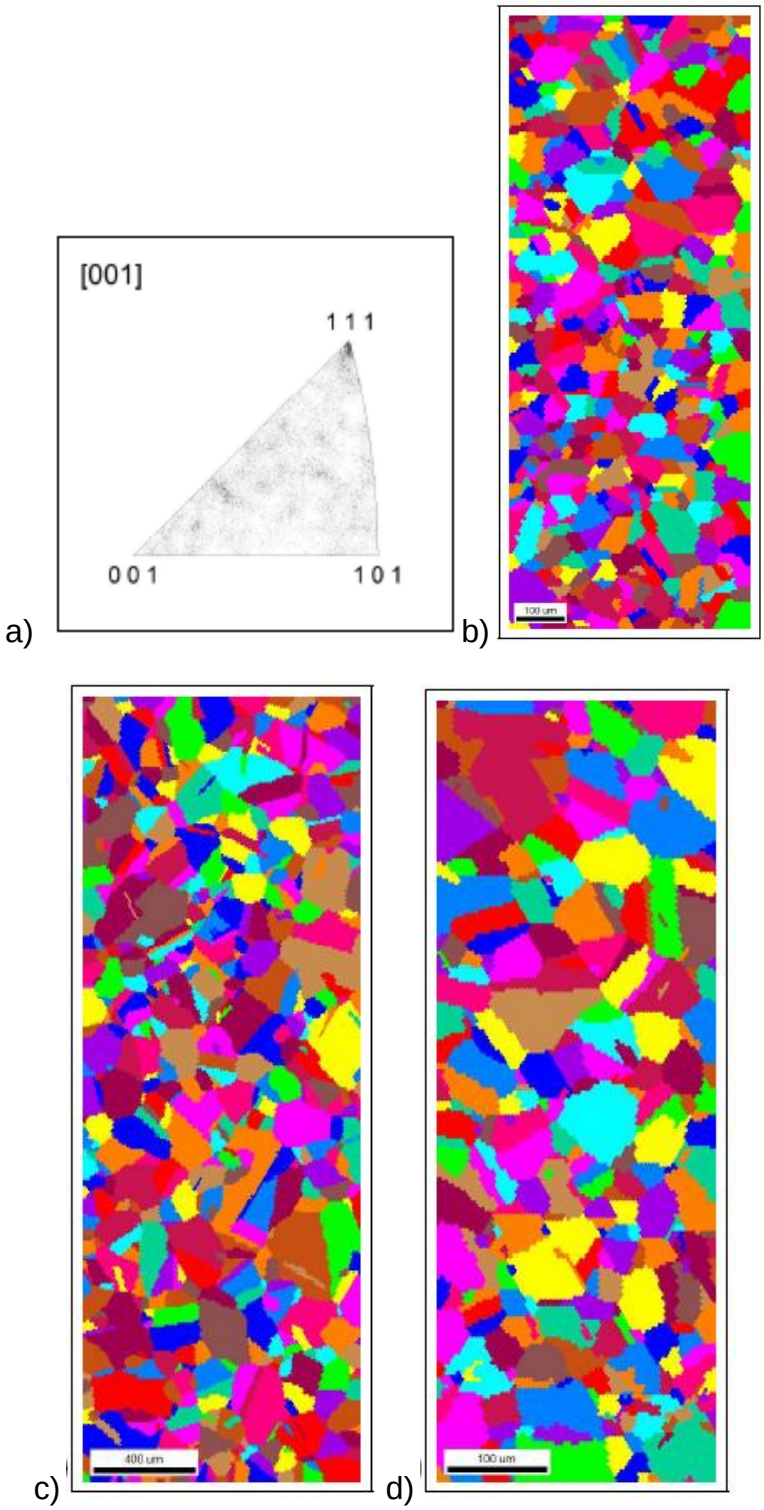

Figure 17. a) IPF of Ni sample annealed at 850°C for 30 mins, b) EBSD image of microstructure of Ni sample annealed at 850°C for 30 mins, c) EBSD image of microstructure of Ni sample annealed at 850°C for 240 mins, d) EBSD image of microstructure of Ni sample annealed at 850°C for 5 mins

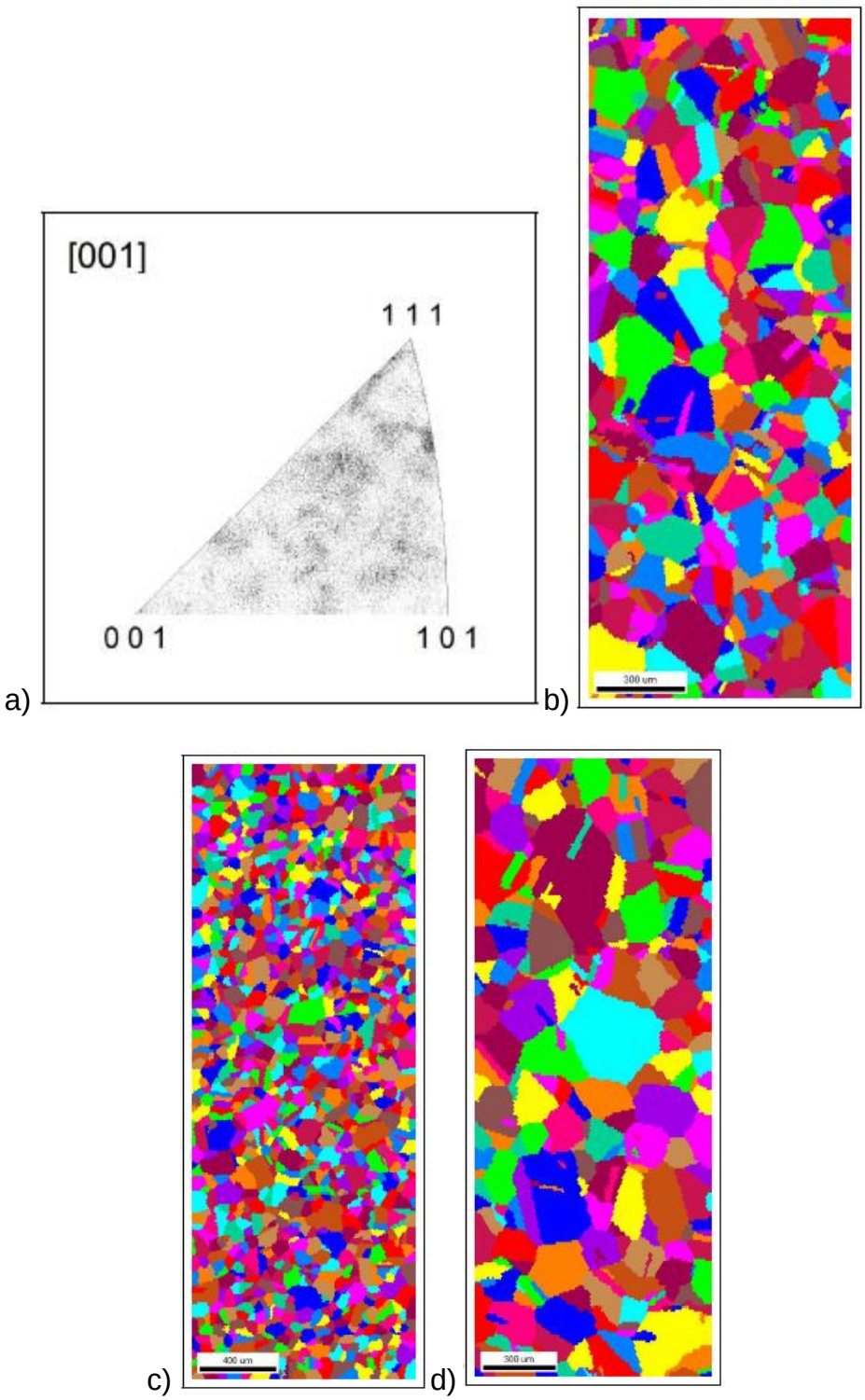

Figure 18. a) IPF of Ni sample annealed at 1000°C for 30 mins, b) EBSD image of microstructure of Ni sample annealed at 1000°C for 30 mins, c) EBSD image of microstructure of Ni sample annealed at 1000°C for 5 mins, d) EBSD image of microstructure of Ni sample annealed at 1000°C for 180 mins

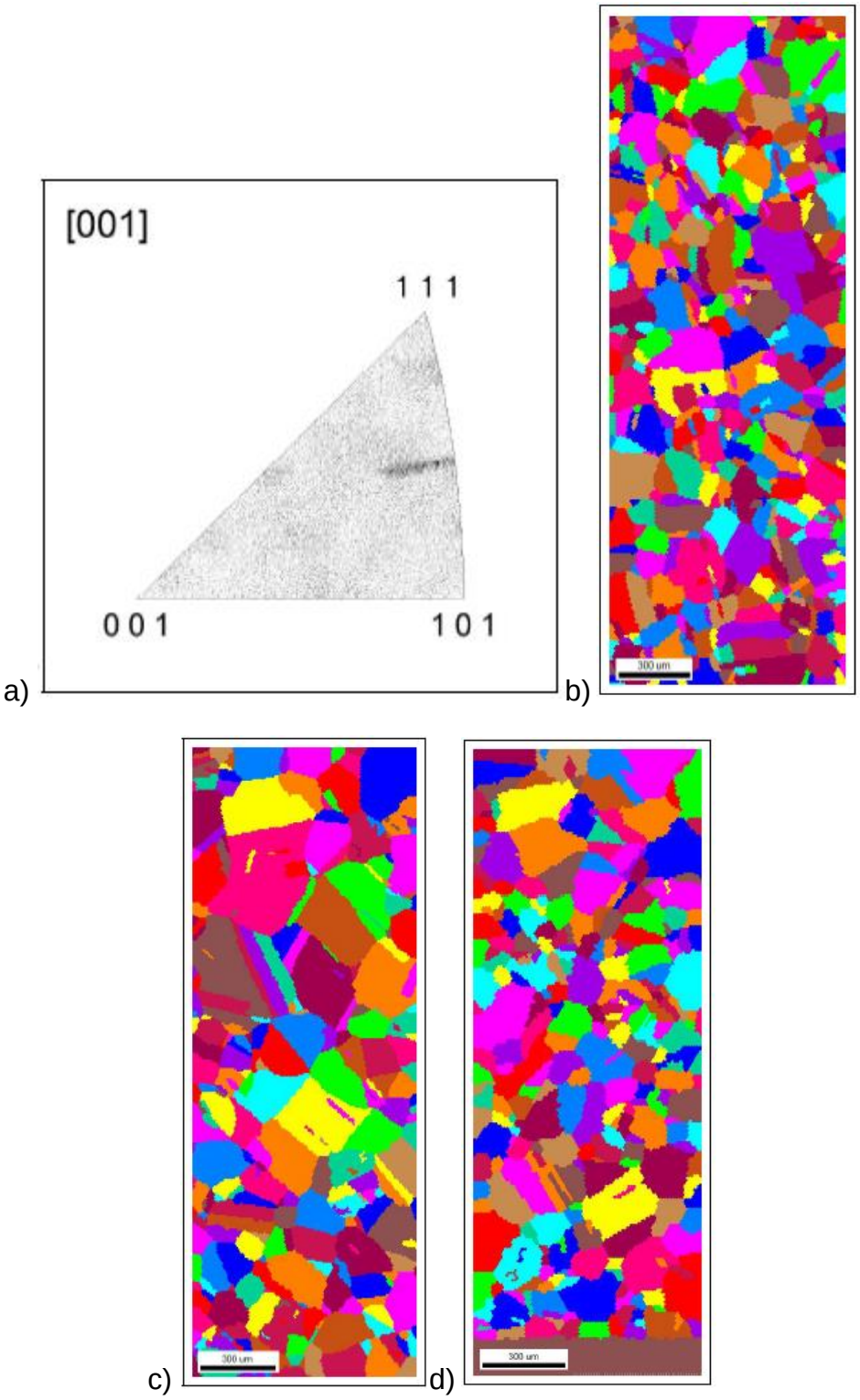

Figure 19. a) IPF of Ni sample annealed at 1100°C for 90 mins, b) EBSD image of microstructure of Ni sample annealed at 1100°C for 90 mins, c) EBSD image of microstructure of Ni sample annealed at 1100°C for 30 mins, d) EBSD image of microstructure of Ni sample annealed at 1100°C for 5 mins

a) 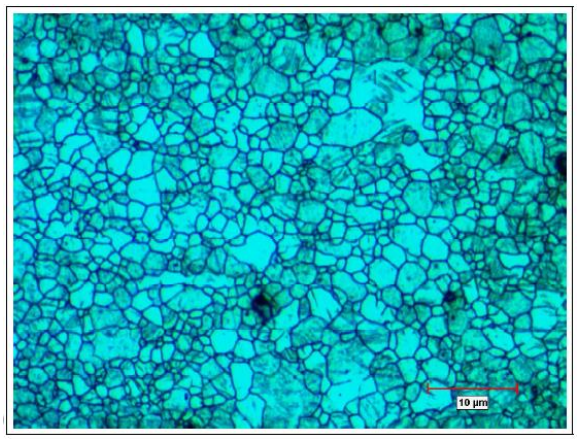 b) 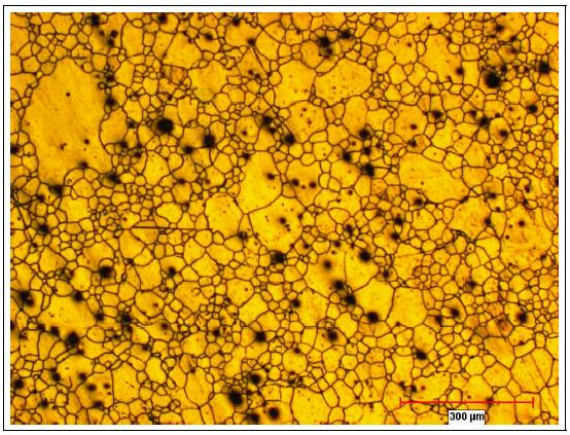

Figure 20. a) and b) shows optical microscope images for AZ31bMg after etching of as-rec and annealed at 450°C for 22 hours

a) 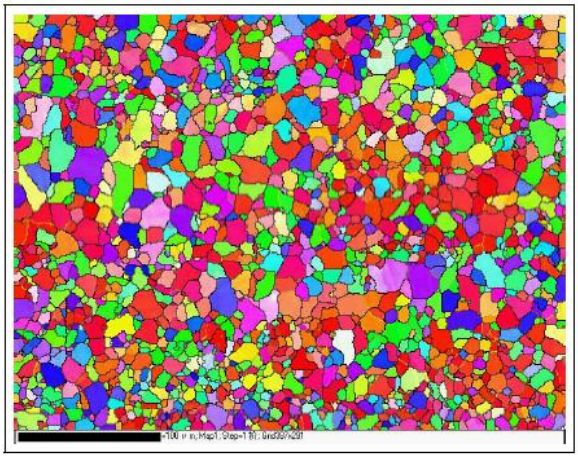 b) 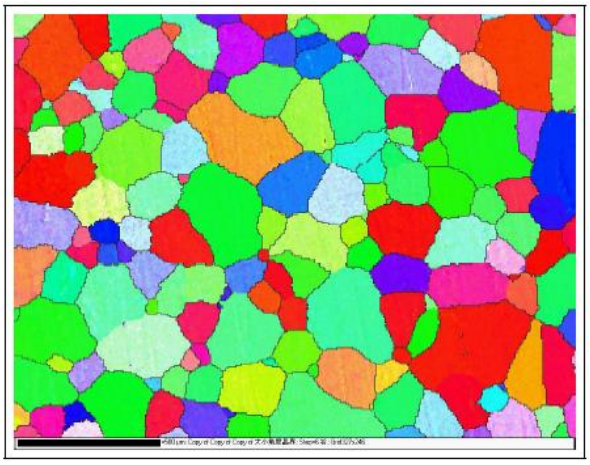

Figure 21. a) and b) shows EBSD images for Al5083F of as-rec and annealed at 600°C for 5 hours

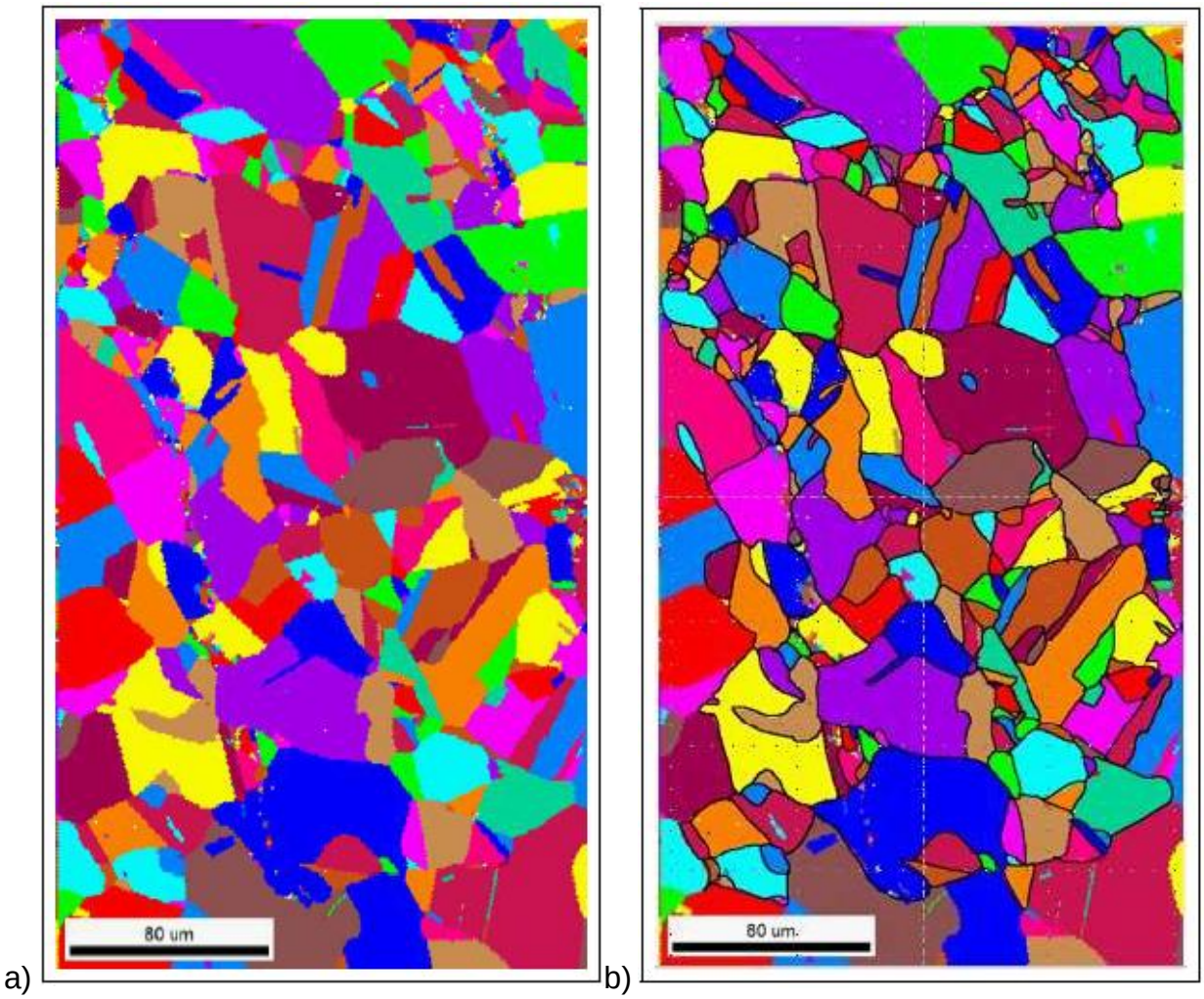

Figure 22. As-received Ni sample a) before tracing, b) highlighted grain boundaries after tracing

Table 5. Summary of all data for Mg, Al and Ni samples

	Average area	Average perim	Temp	Time(s	Time(mir	amin	kbar	S*	Sm
AZ31bMg	3.2252	7.477	25	1		0.25	4.16341	1.44372	0.00173
	9.365	12.47	300	240	4	0.5	4.07486	1.50581	0.00039
	107.253	40.513	300	259200	4320	5	3.91192	1.40394	1.1E-05
	114.655	40.05	300	604800	10080	5	3.7403	1.27256	9.9E-06
	19.4622	17.4565	400	240	4	1	3.95696	1.44633	0.00014
	36.94	23.499	400	3600	60	2	3.86635	1.42098	5.5E-05
	349.7	69.58	400	64800	1080	10	3.7208	1.26402	1.9E-06
	175.018	49.6	450	60	1	10	3.74921	1.35018	5.5E-06
	222.834	53.0344	450	240	4	10	3.55277	1.22296	4.1E-06
	672.67	94.75	450	79200	1320	10	3.65324	1.28319	7.5E-07
A1 5083	56.88	30.62	25	1		2	4.05999	1.37603	2.4E-05
	76.62	34.2	450	3600	1	2	3.9071	1.35033	1.7E-05
	113.15	44.64	500	3600	1	2	4.19659	1.41755	8E-06
	115.75	45.01	500	10800	3	2	4.18358	1.45278	8E-06
	181.74	56.92	550	3600	1	5	4.22221	1.48757	4E-06
	224.63	61.3	550	10800	3	5	4.09003	1.49193	3.2E-06
	7054.89	349.24	600	3600	1	5	4.15795	1.55924	1.8E-08
	18903	562.83	600	18000	5	10	4.09366	1.36177	3.8E-09
Comm pure Ni	186.178	54.7684	25	1		1	4.01389	1.18083	3.6E-06
	397.856	78.729	850	300	5	1	3.94704	1.34833	1.4E-06
	1112.41	125.899	850	1800	30	1	3.77476	1.44829	3.6E-07
	6633.15	306.756	850	14400	240	1	3.76646	1.34129	2.3E-08
	474.6548	86.5634	1000	300	5	1	3.97325	1.27145	9.8E-07
	4176.48	245.626	1000	1800	30	1	3.80075	1.23414	4.2E-08
	8566.19	364.784	1000	10800	180	1	3.94132	1.39525	1.4E-08
	516.873	85.8917	1100	300	5	1	3.77798	1.26188	1E-06
	6786.98	308.239	1100	1800	30	1	3.74153	1.20757	2.1E-08
	19098.98	522.91	1100	5400	90	1	3.78375	1.46186	5.1E-09

APPENDIX C: DERIVATION OF GRAIN SIZE DISTRIBUTIONS

Constraints (26) and (27) select a $2N$ dimensional surface. The area of this phase space is

$$\Gamma_N = \int \delta\left(E - \frac{\Upsilon}{2}\sum_{i=1}^{N} p_i\right)\delta\left(A - \sum_{i=1}^{N} a_i\right)\prod_{i=1}^{N} dp_i \prod_{i=1}^{N} da_i. \quad (41)$$

To find the joint probability distribution of a and p of N^{th} grain, we have to compute the following integral

$$\Gamma_N(a,p) = \int \delta\left(E - \frac{\Upsilon}{2}p - \frac{\Upsilon}{2}\sum_{i=1}^{N-1} p_i\right)\delta\left(A - a - \sum_{i=1}^{N-1} a_i\right)\prod_{i=1}^{N-1} dp_i \prod_{i=1}^{N-1} da_i \quad (42)$$

$$f(a,p) = \frac{\Gamma_N(a,p)}{\Gamma_N}. \quad (43)$$

To begin the computation of integral Γ_N,we represent the delta function as an integral over a line in complex plane

$$\delta(x) = \frac{1}{2\pi i}\int_{b-i\infty}^{b+i\infty} e^{xz} dz.$$

Using the above substitution, eq (41) changes to

$$\Gamma_N = \int e^{zE+\zeta A}\left(\int\int e^{-zp-\zeta a} dp da\right)^N \frac{dz}{2\pi i}\frac{d\zeta}{2\pi i}.$$

$$A = N\bar{a}. \quad (44)$$

$$E = N\gamma\bar{p}. \quad (45)$$

Using assumptions (44) and (45), we get

$$\Gamma_N = \int e^{NS} \frac{dz}{2\pi i} \frac{d\zeta}{2\pi i}. \tag{46}$$

and

$$S(z, \zeta, k, \bar{a}, \bar{p}) = \zeta \bar{a} + z\gamma\bar{p} + lnQ(z, \zeta, k). \tag{47}$$

$$Q(z, \zeta, k) = \int_0^\infty \int_{\frac{kp^2}{4\pi}}^{\frac{p^2}{4\pi}} e^{-z\gamma p - \zeta a} dpda. \tag{48}$$

Following are the proposed change of variables

$$z \to \frac{z}{\gamma\bar{p}}, \zeta \to \frac{\zeta}{\bar{a}}, x = \frac{p}{\bar{p}}, y = \frac{a}{\bar{a}}.$$

This results in eq (48) being transformed to

$$Q(z, \zeta, k, \bar{a}, \bar{p}) = \bar{a}\bar{p} Q_0(z, \zeta, k, \bar{a}, \bar{p}).$$

$$Q_0(z, \zeta, k, \bar{a}, \bar{p}) = \int_0^\infty \int_{\frac{kx^2\bar{p}^2}{4\pi\bar{a}}}^{\frac{x^2\bar{p}^2}{4\pi\bar{a}}} e^{-zx - \zeta y} dxdy. \tag{49}$$

We introduce a new parameter $\varkappa$, which is defined as follows

$$\varkappa = \frac{\bar{p}^2}{4\pi\bar{a}}.$$

This changes only the limits of integration in equation 49 to

$$Q_0(z, \zeta, k, \varkappa) = \int_0^\infty \int_{k\varkappa x^2}^{\varkappa x^2} e^{-zx - \zeta y} dxdy. \tag{50}$$

Integrating eq. 50 w.r.t. y,

$$Q_0(z,\zeta,k,\varkappa) = \frac{1}{\zeta}\int_0^\infty e^{-zx}[e^{-\zeta \mathrm{k}\varkappa \mathrm{x}^2} - e^{-\zeta\varkappa \mathrm{x}^2}]dx. \tag{51}$$

Change of variable

$$\mathrm{x}\sqrt{\zeta k\varkappa} = q, \frac{z}{\sqrt{\zeta}} = t.$$

Hence, eq (51) can be written as

$$Q_0(z,\zeta,k,\varkappa) = \frac{1}{\sqrt{\zeta^3 k\varkappa}}\int_0^\infty e^{-\frac{tq}{\sqrt{k\varkappa}}}\left[e^{-\mathrm{q}^2} - e^{-\frac{\mathrm{q}^2}{k}}\right]dq.$$

$$Q_1(t,k,\varkappa) = \sqrt{\zeta^3 k\varkappa}\,Q_0(t,\zeta,k,\varkappa).$$

$$Q_1(t,k,\varkappa) = \int_0^\infty e^{-\frac{tq}{\sqrt{k\varkappa}}}\left[e^{-\mathrm{q}^2} - e^{-\frac{\mathrm{q}^2}{k}}\right]dq.$$

This changes S in eq (47) to

$$S(t,\zeta,k,\bar{a},\bar{p}) = \zeta + t\sqrt{\zeta} - \frac{3}{2}\ln\zeta - \frac{1}{2}\ln k\varkappa + \ln Q_1(t,k,\varkappa) + \ln \bar{a}\bar{p}.$$

According to steepest descent method, the asymptotics of the integral in eq (46) as $N \to \infty$ is given by the point of minimum of $S(z,\zeta,k,\bar{a},\bar{p})$

$$S(t,\zeta,k,\bar{a},\bar{p}) = \zeta + t\sqrt{\zeta} - \frac{3}{2}\ln\zeta - \frac{1}{2}\ln k\varkappa + \ln Q_1(t,k,\varkappa) + \ln \bar{a}\bar{p}\,.$$

$$Q_1(t,k,\varkappa) = \int_0^\infty e^{-\frac{tq}{\sqrt{k\varkappa}}}[e^{-\mathrm{q}^2} - e^{-\frac{\mathrm{q}^2}{k}}]dq. \tag{52}$$

for real z and ζ. This minimization exercise leads us to values $\check{t}$ and $\check{\zeta}$. $\check{t}$ is the minimizer of S with respect to t for a given value of k and $\varkappa$. Similarly, for ζ.

$$\frac{\partial S}{\partial t} = \sqrt{\zeta} + \frac{1}{Q_1}\frac{\partial Q_1}{\partial t} = 0. \tag{53}$$

$$\frac{\partial S}{\partial \zeta} = 1 + \frac{t}{2\sqrt{\zeta}} - \frac{3}{2\zeta} = 0. \tag{54}$$

When $\varkappa \to \infty$, $\mathrm{k} \to 0$, $Q_1(t,k,\varkappa)$ in eq (52) changes to

$$Q_1(t,k,\varkappa) = \int_0^\infty e^{-\frac{tq}{\sqrt{k\varkappa}}}[e^{-\mathrm{q}^2}]dq.$$

Using Taylor expansion,

$$Q_1(t,k,\varkappa) = \int_0^\infty \left[1 - \frac{tq}{\sqrt{\varkappa k}} + \frac{q^2t^2}{\varkappa k}\right]\left[e^{-q^2}\right]dq.$$

$$Q_1(t,k,\varkappa) = \int_0^\infty e^{-q^2}dq - \frac{t}{\sqrt{\varkappa k}}\int_0^\infty qe^{-q^2}dq + \frac{t^2}{\varkappa k}\int_0^\infty q^2e^{-q^2}dq\,.$$

$$Q_1(t,k,\varkappa) = \frac{\sqrt{\pi}}{2} - \frac{t}{2\sqrt{\varkappa k}} + \frac{\sqrt{\pi}t^2}{4\varkappa k}.$$

To find this asymptotic value of the function and the involved parameters, we will use eqs (53) and (54). This gives us

$$\sqrt{\zeta} = \frac{2\sqrt{\varkappa k}+2\sqrt{\pi}t}{2\varkappa k\sqrt{\pi}-2t\sqrt{\varkappa k}+\sqrt{\pi}t^2}. \tag{55}$$

$$\frac{3}{2\zeta} + \frac{t}{2\sqrt{\zeta}} = 1. \tag{56}$$

If the minimum of S is at $t = 0$, then$\partial S/\partial t \geq 0$ at $t = 0$.Hence, eq (55) gives us an inequality as follows

$$\zeta \geq \frac{1}{\varkappa k \pi} \tag{57}$$

and eq (56) gives

$$\zeta = \frac{3}{2} \tag{58}$$

Combining eqs (57) and (58) we get

$$\varkappa k \geq \frac{2}{3\pi}. \tag{59}$$

In this region defined by inequality (59), $\check{\zeta} = 1.5$, $\check{t} = 0$. Now using eq (43)

$$f(a,p) = ce^{-\check{z}\frac{p}{\bar{p}} - \check{\zeta}\frac{a}{\bar{a}}} \tag{60}$$

where c is normalization constant and $\check{z}$ and $\check{\zeta}$ are determined as shown above. To get $f(p)$ from $f(a,p)$

$$f(p) = \int f(a,p)da.$$

$$\int f(a,p)da\,dp = 1. \tag{61}$$

Therefore, eq (60) yields

$$f(p) = c \int_{\frac{kp^2}{4\pi}}^{\frac{p^2}{4\pi}} e^{-\check{z}\frac{p}{\bar{p}} - \check{\zeta}\frac{a}{\bar{a}}}\, da.$$

$$f\left(\frac{p}{\bar{p}}\right) = c_1 e^{-\check{z}\frac{p}{\bar{p}}}\left[e^{-\check{\zeta}k\varkappa\left(\frac{p}{\bar{p}}\right)^2} - e^{-\check{\zeta}\varkappa\left(\frac{p}{\bar{p}}\right)^2}\right]. \tag{62}$$

where c_1 is given by

$$c_1 = \frac{1}{\int_0^\infty e^{-\check{z}x}\left[e^{-\check{\zeta}k\varkappa x^2} - e^{-\check{\zeta}\varkappa x^2}\right]dx}.$$

To get $f(a)$ from $f(a,p)$

$$f(a) = \int f(a,p)dp.$$

$$\int f(a,p)da\, dp = 1.$$

Therefore, eq (60) yields

$$f(p) = c \int_{\sqrt{4\pi a}}^{\sqrt{\frac{4\pi a}{k}}} e^{-\check{z}\frac{p}{\bar{p}} - \check{\zeta}\frac{a}{\bar{a}}}\, dp.$$

$$f\left(\frac{a}{\bar{a}}\right) = c_1 e^{-\check{\zeta}\frac{a}{\bar{a}}}\left[e^{-\check{z}\sqrt{\varkappa\frac{a}{\bar{a}}}} - e^{-\check{z}\sqrt{\frac{\varkappa a}{k\bar{a}}}}\right]. \tag{63}$$

where c_2 is given by

$$c_2 = \frac{1}{\int_0^\infty e^{-\check{\zeta}x}[e^{-\check{z}\sqrt{\varkappa x}} - e^{-\check{z}\sqrt{\frac{\varkappa x}{k}}}]dx}.$$

APPENDIX D: PROBABILITY DENSITY PLOTS WITH DATA

a) 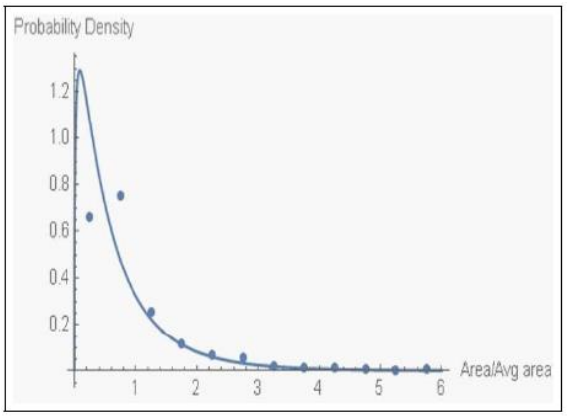

b) 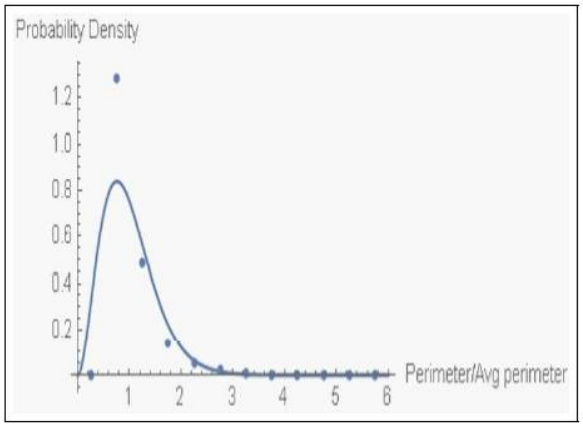

Figure 23. a) Probability density plot for as-rec AZ31bMg microstructure. x-axis is the normalized area and y-axis is the probability density of finding that area in the selected bin. Bin size used is 0.5. b) Probability density plot for as-rec AZ31bMg microstructure. x-axis is the normalized perimeter and y-axis is the probability density of finding that perimeter in the selected bin. Bin size used is 0.5

a) 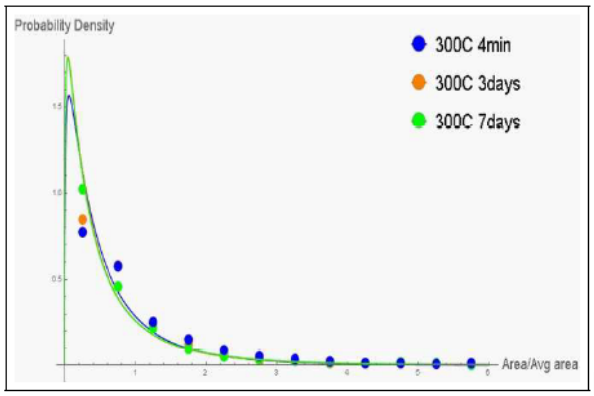

b) 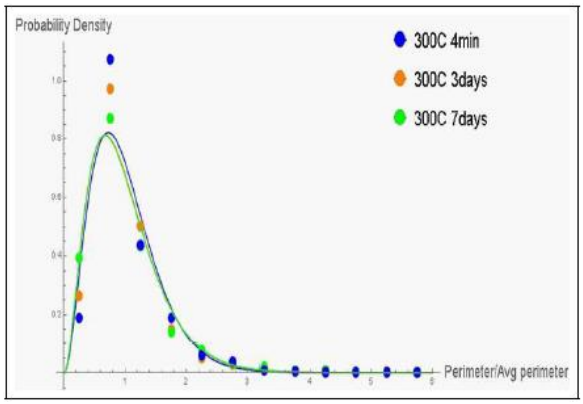

Figure 24. Probability density plot for 300°C annealed AZ31bMg microstructure. a) x-axis is the normalized area and y-axis is the probability density of finding that area in the selected bin. Bin size used is 0.5. b) x-axis is the normalized perimeter and y-axis is the probability density of finding that perimeter in the selected bin. Bin size used is 0.5.

a) 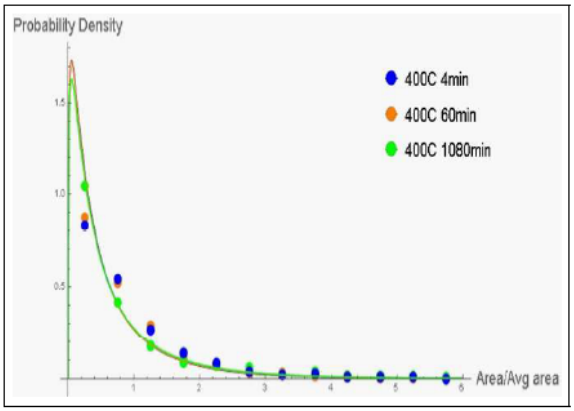

b) 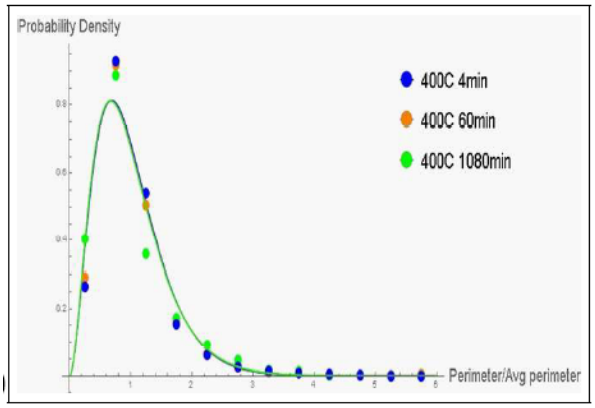

Figure 25. Probability density plot for 400°C annealed AZ31bMg microstructure. a) x-axis is the normalized area and y-axis is the probability density of finding that area in the selected bin. Bin size used is 0.5. b) x-axis is the normalized perimeter and y-axis is the probability density of finding that perimeter in the selected bin. Bin size used is 0.5.

a) 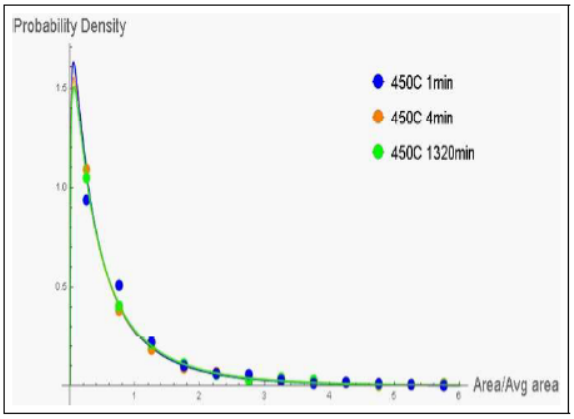

b) 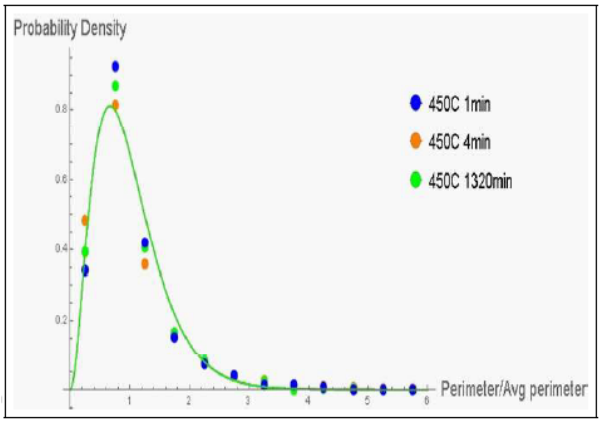

Figure 26. Probability density plot for 450°C annealed AZ31bMg microstructure. a) x-axis is the normalized area and y-axis is the probability density of finding that area in the selected bin. Bin size used is 0.5. b) x-axis is the normalized perimeter and y-axis is the probability density of finding that perimeter in the selected bin. Bin size used is 0.5.

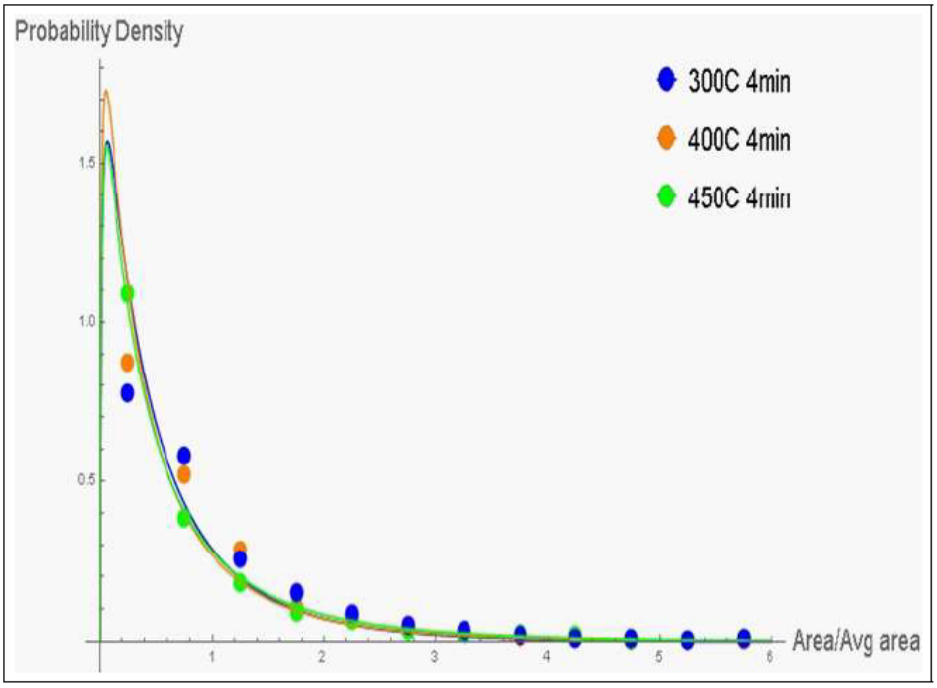

Figure 27. Probability density plot for 4 min annealed AZ31bMg microstructure. x-axis is the normalized area and y-axis is the probability density of finding that area in the selected bin. Bin size used is 0.5

Table 6. Summary of all the data for AZ31b Mg samples

Temp (C)	Time (min)	Mean area (um^2)	Mean per (um)	kappa	a0	N*	S*	Sm
As Rec		3.2252	7.477	1.3788	0.25	3101	3.557	11030
300	4	9.365	12.47	1.3208	0.5	1068	3.93	4197
300	4320	107.253	40.513	1.2173	5	93.2	4.066	379.1
300	10080	114.655	40.05	1.1128	5	87.2	4.132	360.4
400	4	19.4622	17.4565	1.2455	1	514	3.968	2039
400	60	36.94	23.499	1.1891	2	271	3.916	1060
400	1080	349.7	69.58	1.1013	10	28.6	4.554	130.2
450	1	175.018	49.6	1.1181	10	57.1	3.862	220.7
450	4	222.834	53.0344	1.004	10	44.9	4.104	184.2
450	1320	672.67	94.75	1.0616	10	14.9	5.209	77.43

REFERENCES

[1] Ferry M., Humphreys F.J., Discontinuous subgrain growth in deformed and annealed {110}<001> aluminium single crystals.*Acta Materialia*. **44**,1293-1308 (1996).

[2] Kinderlehrer D., Livshits I., S. Ta'Asan, A variational approach to modeling and simulation of grain growth.*Siam J Sci Comput*. **28**, 1694-1715 (2006).

[3] Klement W., Willens R.H., Duwez P., Non-Crystalline Structure in Solidified Gold-Silicon Alloys.*Nature*. **187**, 869-870 (1960).

[4] Tucker J.C., Chan L.H., Rohrer G.S., Groeber M.A., Rollett A.D., Comparison of grain size distributions in a Ni-based superalloy in three and two dimensions using the Saltykov method.*Scripta Materialia*. **66**, 554-557 (2012).

[5] Forsyth P.J.E., King R., Metcalfe G.J., Chalmers B., Grain Boundaries in Metals.*Nature*. **158**, 875-876 (1946).

[6] AU Evans, U.R., The laws of expanding circles and spheres in relation to the lateral growth of surface films and grain size of metals.*Transactions of the Faraday Society*. **41**, 365-374 (1945).

[7] Burke, J.E., Turnbull, D., Recrystallization and grain growth.*Progress in Metal Physics*. **3**, 220-292 (1952).

[8] Galiyev, A., Kaibyshev, R., Gottstein, G., Correlation of plastic deformation and dynamic recrystallization in magnesium alloy Zk60.*Acta Materialia*. **49**, 1199-1207 (2001).

[9] Yu, Q., Esche, S.K., A Monte Carlo algorithm for single phase normal grain growth with improved accuracy and efficiency.*Computational Materials Science*. **27**, 259-270 (2003).

[10] Zollner, D., A Potts model for junction limited grain growth.*Computational Materials Science*. **50**, 2712-2719 (2011).

[11] Nordbakke, M.W., Ryum, N., Hunderi, O., Curvilinear polygons, finite circle packings, and normal grain growth.*Materials Science and Engineering A-Structural Materials Properties, Microstructure and processing*. **385**, 229-234 (2004).

[12] Zhang, C., Suzuki, A., Ishimaru, T., Enomoto, M., Characterization of three-dimensional grain structure in polycrystalline iron by serial sectioning.*Metallurgical and Materials Transactions A- Physical Metallurgy and Materials Science*. **35A**, 1927-1933 (2004).

[13] Petrov, I., Barna, P.B., Hultman, L., Greene, J.E., Microstructural evolution during film growth.*Journal of Vaccum Science and Technology A*. **21**, S117-S128 (2003).

[14] Wang, H., Liu, G.Q., Qin, X.G., Grain size distribution and topology in 3D grain growth simulation with large-scale Monte Carlo method.*International Journal of Minerals Metallurgy and Materials*. **16**, 37-42 (2009).

[15] Michalak, J.T., Paxton, H.W., Some recovery characteristics of zone-melted iron.*Transactions of the Metallurgical Society of AIME*. **221**, 850-857 (1961).

[16] Furu T., Ørsund R., Nes E., Subgrain growth in heavily deformed aluminium---experimental investigation and modelling treatment.*Acta Metallurgica et Materialia*. **43**, 2209-2232 (1995).

[17] Vandermeer, R.A., Hansen, N., Recovery kinetics of nanostructured aluminum: Model and experiment.*Acta Materialia*. **56**, 5719-5727 (2008).

[18] Driver, J.H., Stability of nanostructured metals and alloys.*Scripta Materialia*. **51**, 819-823 (2004).

[19] Humphreys, F. J., Hatherly, M., Recrystallization and related annealing phenomena. *Elsevier* (2012).

[20] Edwards, S.F., The rheology of powders.*Rheologica Acta*. **29**, 493-499 (1990).

[21] Edwards, S.F., The aging of glass forming liquids.*Disorder in condensed matter physics: A volume in honor of R. Elliott*. 147-154 (1991).

[22] Edwards, S.F., The role of entropy specifications of powder in Granular Matter: an Interdisciplinary Approach (ed. Mehta A), pp.121--140 (*Springer-Verlag*, 1994).

[23] Bouchbinder, E., Langer, J.S., Nonequilibrium thermodynamics of driven amorphous materials.I. Internal degrees of freedom and volume deformation.*Physical Review E*.**80 - 031131** (2009).

[24] Bouchbinder, E., Langer, J.S., Nonequilibrium thermodynamics of driven amorphous materials.II. Effective-temperature theory.*Physical Review E*. **80 - 031132** (2009).

[25] Bouchbinder, E., Langer, J.S., Nonequilibrium thermodynamics of driven amorphous materials.III.Shear-transformation-zone plasticity.*Physical Review E*. **80 - 031133** (2009).

[26] Bouchbinder, E., Langer, J.S., Procaccia, I., Athermal shear-transformation-zone theory of amorphous plastic deformation. I. Basic principles.*Physical Review E*. **75 - 036107** (2007).

[27] Falk, M.L., Langer, J.S., Dynamics of viscoplastic deformation in amorphous solids.*Physical Review E*. **57**, 7192-7205 (1998).

[28] Falk, M.L., Langer, J.S., Deformation and Failure of Amorphous, Solidlike Materials.*Annual Review of Condensed Matter Physics*. **2**, 353-373 (2011).

[29] Haxton, T.K., Liu, A.J., Activated dynamics and effective temperature in a steady state sheared glass.*Physical Review Letters*. **99 - 195701** (2007).

[30] Langer, J.S., Shear-transformation-zone theory of plastic deformation near the glass transition.*Physical Review E*. **77 - 021502** (2008).

[31] Langer, J.S., Manning, M.L., Steady-state, effective-temperature dynamics in a glassy material.*Physical Review E*. **76 - 056107** (2007).

[32] Nieuwenhuizen, T.M., Thermodynamics of the glassy state: Effective temperature as an additional system parameter.*Physical Review Letters*. **80**, 5580-5583 (1998).

[33] O'Hern, C.S., Liu, A.J., Nagel, S.R., Effective temperatures in driven systems: Static versus time-dependent relations.*Physical Review Letters*. **93 - 165702** (2004).

[34] Ono, I.K. et.al., Effective temperatures of a driven system near jamming.*Physical Review Letters*. **89 - 095703** (2002).

[35] Potiguar, F.Q., Makse, H.A., Effective temperature and jamming transition in dense, gently sheared granular assemblies.*European Physical Journal E*. **19**, 171-183 (2006).

[36] Cugliandolo, L.F., Kurchan, J., Peliti, L., Energy flow, partial equilibration, and effective temperatures in systems with slow dynamics.*Physical Review E*. **55**, 3898-3914 (1997).

[37] Sollich, P. et.al, Rheology of soft glassy materials.*Physical Review Letters*. **78**, 2020-2023 (1997).

[38] Berdichevsky, V.L., Homogenization in micro-plasticity.*Journal of Mechanics and Physics of Solids*. **53**, 2457-2469 (2005).

[39] Berdichevsky, V.L., On thermodynamics of crystal plasticity.*Scripta Materialia*. **54**, 711-716 (2006).

[40] Berdichevsky, V.L., A continuum theory of edge dislocations.*Journal of Mechanics and Physics of Solids*. **106**, 95-132 (2007)

[41] Langer, J.S., Bouchbinder, E., Lookman, T., Thermodynamic theory of dislocation-mediated plasticity.*Acta Materialia*. **58**, 3718-3732 (2010)

[42] Langer, J.S., Statistical thermodynamics of strain hardening in polycrystalline solids.*Physical Review E*. **92 - 032125** (2015).

[43] Le, K.C., Thermodynamic dislocation theory for non-uniform plastic deformations.*Journal of Mechanics and Physics of Solids*. **111**, 157-169 (2018).

[44] Berdichevsky, V.L., Entropy of microstructure.*Journal of Mechanics and Physics of Solids*. **56**, 742-771 (2008).

[45] Barmak, K., Eggeling, E., Emelianenko, M., Epshteyn, Y., Kinderlehrer, D., Sharp, R., Ta'asan, S., An entropy based theory of the grain boundary character distribution.*Discrete and Continuous Dynamical Systems*. **30**, 427-454 (2011).

[46] Barmak, K., Eggeling, E., Emelianenko, M., Epshteyn, Y., Kinderlehrer, D., Sharp, R., Ta'asan, S., Critical events, entropy, and the grain boundary character distribution.*Physical Review B*. **83**, (2011).

[47] Berdichevsky, V.L., Thermodynamics of microstructure evolution: Grain growth.*International Journal of Engineering Science*. **57**, 50-78 (2012).

[48] Berdichevsky, V.L., Beyond classical thermodynamics: grain growth.*Emerging Materials Research*. **2**, 66-70 (2013)

[49] Berdichevsky, V.L., Variational Principles of Continuum Mechanics.(*Springer*, 2009).

[50] Arnold, V.I., Kozlov, V.V., Neishtadt, A.I., Mathematical aspects of classical and celestial mechanics, v.3 of Encycl. of Math Sciences. (*Springer*, 1988)

[51] Berdichevsky, V.L., Entropy and temperature of microstructure in crystal plasticity.*International Journal of Engineering Science*. **128**, 24-30 (2018).

[52] Berdichevsky, V.L., Beyond classical thermodynamics: dislocation mediated plasticity.*Journal of Mechanics and Physics of Solids*. **129**, 83-118 (2019)

[53] Von Neumann, J., Metal Interfaces. (Am. Soc. Metals, Cleveland, 1952), pp.108--110.

[54] Smith, C. S., Metal Interfaces. (Am. Soc. Metals, Cleveland, 1952), pp.65--108.

[55] Mullins, W.W., 2-dimensional motion of idealized grain boundaries.*Journal of Applied Physics*. **27**, 900-904 (1956).

[56] Kinderlehrer, D., Liu, C., Evolution of grain boundaries.*Mathematical Models and Methods in Applied Sciences*. **11**, 713-729 (2001).

[57] Anderson, M.P., Srolovitz, D.J., Grest, G.S., Sahni, P.S., Computer-Simulation of Grain-Growth 1.Kinetics.*Acta Metallurgica*. **32**, 783-791 (1984).

[58] Srolovitz, D.J., Anderson, M.P., Sahni, P.S., Grest, G.S., Computer-Simulation of Grain-Growth 2.Grain-size Distribution, Topology, and Local Dynamics.*Acta Metallurgica*. **32**, 793-802 (1984).

[59] Anderson, M.P., Grest, G.S., Srolovitz, D.J., Computer-Simulation of Normal Grain-Growth in 3 dimensions.*Philosophical Magazine B-Physics of Condensed Matter Statistical Mechanics Electronic Optical and Magnetic Properties*. **59**, 293-329 (1989).

[60] Han, J., Thomas, S.L., Srolovitz, D.J., Grain-boundary kinetics: A unified approach.*Progress in Materials Science*. **98**, 386-476 (2018).

[61] Doherty, R.D., Hughes, D.A., Humphreys, F.J., Jonas, J.J., Juul Jensen, D., Kassner, M.E., King, W.E., McNelley, T.R., McQueen, H.J., Rollett, A.D., Current issues in recrystallization: a review.*Materials Science and Engineering A-Structural Materials Properties-Microstructure and Processing*. **238**, 219-274 (1997).

[62] Humphreys, F.J., A unified theory of recovery, recrystallization and grain growth, based on the stability and growth of cellular microstructures .1.The basic model.*Acta Materialia*. **45**, 4231-4240 (1997).

[63] Fan, D., Chen, L.Q., Computer simulation of grain growth using a continuum field model.*Acta Materialia*. **45**, 611-622 (1997).

[64] Holm, E. A., Foiles, S. M., How Grain Growth Stops: A Mechanism for Grain-Growth Stagnation in Pure Materials.*Science*. **328**, 1138-1141 (2010).

[65] Berdichevsky, V.L., A new statistical model for 2D grain size distribution (Unpublished).

[66] Hillert, M., On Theory of Normal and Abnormal Grain growth.*Acta Metallurgica*. **13**, 227 (1965).

[67] Louat, N.P., Theory of normal grain-growth.*Acta Metallurgica*. **22**, 721-724 (1974).

[68] Pande, C. S., On stochastic theory of grain growth.*Acta Metallurgica*. **35**, 2671--2678 (1987).

[69] Atkinson, H.V., Theories of normal grain-growth in pure single-phase systems.*Acta Metallurgica*. **36**, 469-491 (1988).

[70] Berdichevsky, V.L., Universal grain size distribution, most chaotic microstructures and tessellation condition.*International Journal of Engineering Science*. **57**, 24-35 (2012).

[71] Wu, H., Private communication

[72] Bhattacharyya, J.J.,Agnew, S.R. ,Muralidharan, G. , Texture enhancement during grain growth of magnesium alloy AZ31B.*Acta Materialia*. **86**, 80-94(2015).

[73] Pólya, G., and Szegö, G.,"Tables" in Isoperimetric Inequalities in Mathematical Physics (AM-27), (*Princeton University Press*, 1951).

[74] Phillips, H.W.L., The grain size of rolled aluminium.*Journal of the Institute of Metals*. **68**, 47--108 (1942).

[75] Tomkeieff, S.I., Linear intercepts, Areas and Volumes. *Nature*. **155**, 24 (1945).

[76] Smith, C.S., Guttman, L., Measurement of internal boundaries in 3-dimensional structures by random sectioning.*Transactions of the American Institute of Mining and Metallurgical Engineers*. **197**, 81-87 (1953).

[77] McLean, D., Grain Boundaries in Metals, (*Clarendon Press*, 1957).

[78] Dehoff, R.T., Rhines, F.N., Quantitative Microscopy, (*McGraw-Hill*,1968).

[79] Underwood, E.E., Quantitative Stereology 2nd ed. (*Addison-Wesley Publishing Company*, 1970).

[80] Saltikov, S.A., Stereology, ed. H. Elias, (*Springer*,1970).

[81] Glazier, J.A., Grain-Growth in 3 Dimensions Depends on Grain Topology.*Physical Review Letters.* **70**, 2170-2173 (1993).

[82] Saylor, D.M., El Dasher, B.S., Rollett, A.D., Rohrer, G.S., Distribution of grain boundaries in aluminum as a function of five macroscopic parameters.*Acta Materialia*. **52**, 3649-3655 (2004).

[83] Barmak, K., Eggeling, E., Kinderlehrer, D., Sharp, R., Ta'asan, S., Rollett, A.D., Coffey K.R., Grain growth and the puzzle of its stagnation in thin films: The curious tale of a tail and an ear.*Progress in Material Science*. **58**, 987-1055 (2013).

[84] Humphreys, F.J., Review - Grain and subgrain characterisation by electron backscatter diffraction.*Journal of Materials Science*. **36**, 3833-3854 (2001).

[85] Zou, Y., Qin, W., Irissou, E., Legoux, J.G., Yue, S., Szpunar, J.A., Dynamic recrystallization in the particle/particle interfacial region of cold-sprayed nickel coating: Electron backscatter diffraction characterization.*Scripta Materialia*. **61**, 899-902 (2009).

[86] Yu, T.B., Hansen, N., Huang, X.X., Linking recovery and recrystallization through triple junction motion in aluminum cold rolled to a large strain.*Acta Materialia*. **61**, 6577-6586 (2013).

[87] Gottstein, G., Shvindlerman, L. S., Grain boundary migration in metals: thermodynamics, kinetics, applications. *CRC press* (2009).

[88] Hughes, D.A., Hansen, N., Microstructure and strength of nickel at large strains.*Acta Materialia*. **48**, 2985-3004 (2000).

[89] Huang, Y., Humphreys, F.J., Ferry, M., The annealing behaviour of deformed cube-oriented aluminium single crystals.*Acta Materialia*. **48**, 2543-2556 (2000).

[90] Huang, Y., Humphreys, F.J., Subgrain growth and low angle boundary mobility in aluminium crystals of orientation {110}{001}.*Acta Materialia*. **48**, 2017-2030 (2000).

[91] Vandermeer, R.A., Jensen, D.J., Quantifying Recrystallization Nucleation and Growth-Kinetics of cold-worked copper by microstructural analysis.*Metallurgical and Materials Transactions A- Physical Metallurgy and Materials Science*. **26**, 2227-2235 (1995).

[92] Vandermeer, R.A., Jensen, D.J., Microstructural path and temperature dependence of recrystallization in commercial aluminum.*Acta Materialia*. **49**, 2083-2094 (2001).

[93] Grey, E.A., Higgins, G.T., Solute limited grain-boundary migration - A rationalization of grain growth.*Acta Matellurgica*. **21**, 309-321 (1973).

ABSTRACT

STUDY OF GRAIN GROWTH IN SINGLE-PHASE POLYCRYSTALS

by

PAWAN VEDANTI

December 2020

Advisors: Dr. Victor Berdichevsky, Dr. Xin Wu

Major: Mechanical Engineering

Degree: Doctor of Philosophy

Materials with random microstructure are characterized by additional thermodynamic parameters, entropy and temperature of microstructure. It has been argued that there is one more law of thermodynamics: entropy of microstructure decays in isolated systems. This assertion has been checked experimentally for the process of grain growth which showed that entropy of grain structure decays indeed as expected. The equation of state for microstructure entropy has also been studied. In general, entropy of grain microstructure is expected to be a function of grain structure energy and the average grain size. Our experiments suggest that in fact the equation of state degenerates and microstructure entropy becomes a function of either grain energy or grain volume. This follows from an unexpected by-product of the experiments, a seemingly universal relationship between grain volume and grain area, at least at the stage of self-similar grain growth. In addition, a statistical model containing two new characteristics of grain structure in pure metals and alloys is suggested. Non-equiaxed

geometry of grains and grain structure are quantified by using new statistical characteristics. The equations for probability distribution of grain sizes are derived in terms of these parameters. It describes the previously obtained experimental data reasonably well. Evolution of grain size distribution and the above mentioned parameters have been studied during grain growth.

AUTOBIOGRAPHICAL STATEMENT

- 1992 – Born in Shimoga, Karnataka, INDIA
- 2010 – Graduated high school in G.D. Sawant College, Nashik
- 2014 – B.E. in mechanical engineering from Maharashtra Institute of Technology, University of Pune, Pune.
- 2016 – M.S. in mechanical engineering, Wayne State University, Detroit.
- 2020 – Ph.D. in mechanical engineering, Wayne State University, Detroit.